

## Electronic Supporting Information

# Boron,Nitrogen-Containing Heterocyclic Carbene (BNC) as a Redox Active Ligand: Synthesis and Characterization of a Lithium (BNC-)Aurate Complex

Yoshitaka Kimura,<sup>a</sup> Leonardo I. Lugo-Fuentes,<sup>b</sup> Souta Saito,<sup>a</sup> J. Oscar C. Jimenez-Halla,<sup>b</sup> Joaquín Barroso-Flores,<sup>c</sup> Yohsuke Yamamoto,<sup>a</sup> Masaaki Nakamoto,<sup>a</sup> and Rong Shang<sup>a\*</sup>

**Abstract:** Stabilization of low oxidation gold anions as aurate or auride by organic ligands has long been a synthetic challenge, owing to the proneness for low-valent gold centers to cluster. Despite being the most electronegative metal, isolable gold(I) aurate complexes has been only obtained from a few  $\sigma$ -withdrawing organo- and organo-main group ligands. Stabilization of highly-reduced gold complexes by  $\pi$ -modulating redox active ligand has only been achieved by cyclic (amino)(alkyl)carbene (CAAC), which limits to  $1e^-$ -reduction to form neutral gold(0) complexes. This work reports a simple modular synthesis of a boron, nitrogen-containing heterocyclic carbene (<sup>c</sup>BNC) at a gold(I) center through metal-assisted coupling between azadiboriridine and isocyanides. The anionic electrophilic <sup>c</sup>BNC ligand in gold(I) complex [<sup>c</sup>BNC]AuPMe<sub>3</sub> (**3a** and **3b**) allows an  $2e^-$ -reduction to form the first  $\eta^1$ -carbene aurate complex [(BNC)AuPMe<sub>3</sub>]Li(DME) (**5a**, DME=dimethoxyethane). Single crystal crystallographic analysis and computational studies of these complexes revealed a highly  $\pi$ -withdrawing character in the neutral  $4\pi$  B,N-heterocyclic carbene (BNC) moiety and its reduced form showed a  $6\pi$  weakly aromatic character with  $\pi$ -donating properties to the gold(I) fragment, showcasing the first cyclic carbene ligand that allows electronic tunability between  $\pi$ -withdrawing (Fischer-type)- and  $\pi$ -donating (Schrock-type) properties.

---

## Table of Contents

<b>Experimental Procedures</b> .....	<b>2</b>
<b>General Considerations</b> .....	<b>2</b>
<b>Preparation of 3a and 3b</b> .....	<b>2</b>
<b>Preparation of 4a and 4b</b> .....	<b>3</b>
<b>Preparation of 5a</b> .....	<b>3</b>
<b>Crystallographic Studies (3a/b, 4a and 5a)</b> .....	<b>3</b>
<b>General Considerations</b> .....	<b>3</b>
<b>Computational Details</b> .....	<b>5</b>
<b>References</b> .....	<b>18</b>
<b>Appendix I -NMR spectra</b>	

## Experimental Procedures

### General Considerations

All syntheses were carried out under inert atmosphere with standard Schlenk and glovebox techniques unless otherwise stated. Inert gases (both N<sub>2</sub> and Ar) were passed through a dry column of P<sub>2</sub>O<sub>5</sub>. Tetrahydrofuran (THF), diethylether (Et<sub>2</sub>O), Dimethoxyethane (DME), hexane and toluene were freshly distilled from Na/benzophenone prior to use. C<sub>6</sub>D<sub>6</sub> and Tol-*d*<sub>8</sub> were distilled from sodium and degassed three times using freeze-pump-thaw cycling and stored in an argon-filled glovebox. Compounds **1**<sup>S1</sup> and **2**<sup>S2</sup> were prepared according to the literature procedures. The isocyanides CNtBu and CNCy were purchased from Sigma-Aldrich and used without further purification. Other chemicals were used as supplied. <sup>1</sup>H NMR (400 MHz) <sup>11</sup>B{<sup>1</sup>H} NMR (128 MHz), and <sup>31</sup>P{<sup>1</sup>H} NMR (162 MHz) were recorded using a JEOL AL-400 spectrometer, JNM-ECA 500 NMR spectrometer [<sup>1</sup>H NMR (500 MHz), <sup>2</sup>H NMR (92 MHz), <sup>13</sup>C{<sup>1</sup>H} NMR (126 MHz), <sup>11</sup>B{<sup>1</sup>H} NMR (160 MHz) and <sup>31</sup>P{<sup>1</sup>H} NMR (202 MHz)] or JEOL JNM-ECA 600 NMR spectrometer [<sup>1</sup>H NMR (600 MHz), <sup>11</sup>B{<sup>1</sup>H} NMR (193 MHz), and <sup>31</sup>P{<sup>1</sup>H} NMR (243 MHz)]. Chemical shift (δ) are given in ppm with reference against external SiMe<sub>4</sub> (<sup>1</sup>H, <sup>13</sup>C{<sup>1</sup>H}), BF<sub>3</sub>·Et<sub>2</sub>O (<sup>11</sup>B) and 85% H<sub>3</sub>PO<sub>4</sub> (<sup>31</sup>P). High-resolution mass spectra (HRMS) were recorded with a Thermo Fischer Scientific samples.

### Preparation of 3a and 3b

**3a:** Compound **2** (82.7 mg, 0.160 mmol) and the cyclohexyl isocyanide CyNC (13.3 mg, 0.160 mmol) were dissolved in cold toluene (ca. -30 °C, 2-3 mL) separately and then mixed together. After shaking by hand for 10 minutes, the reaction mixture was filtered through a cotton plug. The collected filtrate was pumped to yield the crude product as a yellow solid. Washing with pentane 3 times afforded **3a** as a white solid (95 mg, 0.152 mmol, 95%). <sup>1</sup>H NMR (600 MHz, C<sub>6</sub>D<sub>6</sub>): δ 1.85 (NC(CH<sub>3</sub>)<sub>3</sub>, s, 9H), 1.77 (BC(CH<sub>3</sub>)<sub>3</sub>, s, 9H), 1.38 (BC(CH<sub>3</sub>)<sub>3</sub>, s, 9H), 0.58 (P(CH<sub>3</sub>)<sub>3</sub>, d, <sup>2</sup>J<sub>PH</sub> = 6 Hz, 9H). <sup>11</sup>B NMR (193 MHz, C<sub>6</sub>D<sub>6</sub>): δ 42.1 (s), 11.2 (s). <sup>31</sup>P NMR (243 MHz, C<sub>6</sub>D<sub>6</sub>): δ 1.44. <sup>13</sup>C{<sup>1</sup>H} NMR (100 MHz, C<sub>6</sub>D<sub>6</sub>): δ 251.3 (AuC), 61.8 (s, NCH), 53.6 (s, NC(CH<sub>3</sub>)<sub>3</sub>), 36.5 (s, (B)(B)NC(CH<sub>3</sub>)<sub>3</sub>), 37.62, 35.0, 27.1, 27.0, 26.9 (s, Cy), 32.9 (s, B(Cl)C(CH<sub>3</sub>)<sub>3</sub>), 30.7 (s, BC(CH<sub>3</sub>)<sub>3</sub>), 23.7 (br, BC(CH<sub>3</sub>)<sub>3</sub>), 22.8 (br, BC(CH<sub>3</sub>)<sub>3</sub>), 14.7 (d, P(CH<sub>3</sub>)<sub>3</sub>, <sup>1</sup>J<sub>PC</sub> = 33 Hz). MS-ESI(+): found. 589.33378 [M-Cl]<sup>+</sup>, calcd. 589.33308.

**3b:** Hexane (4.0 mL) solution of *t*BuNC (3.2 mg, 38.5 μmol) was added to a Et<sub>2</sub>O (2.0 mL) solution of **2** (13.3 mg, 25.8 μmol) at ca. -30 °C. The reaction mixture was stirred for 5 minutes at room temperature before filtered through a cotton plug. The cotton plug was then washed with hexane. The combined filtrate was concentrated and stored at -30 °C to afford colorless crystals of **3b**. <sup>1</sup>H NMR (600 MHz, toluene-*d*<sub>6</sub>): δ 2.12 (NC(CH<sub>3</sub>)<sub>3</sub>, s, 9H), 1.81 (NC(CH<sub>3</sub>)<sub>3</sub>, s, 9H), 1.76 (BC(CH<sub>3</sub>)<sub>3</sub>, s, 9H), 1.26 (B(Cl)C(CH<sub>3</sub>)<sub>3</sub>, s, 9H), 0.60 (P(CH<sub>3</sub>)<sub>3</sub>, <sup>2</sup>J<sub>PH</sub> = 12 Hz). To slow down decomposition of **3b** in solution, <sup>13</sup>C{<sup>1</sup>H} and 2D NMR measurements were carried out at lower temperatures. <sup>13</sup>C{<sup>1</sup>H} NMR (150 MHz, toluene-*d*<sub>8</sub>, -38 °C): 258.3 (AuC), 63.8 (s, NC(CH<sub>3</sub>)<sub>3</sub>), 52.2 (s, NC(CH<sub>3</sub>)<sub>3</sub>), 37.6 (s, (B)(B)NC(CH<sub>3</sub>)<sub>3</sub>), 34.9 (br, (C)NC(CH<sub>3</sub>)<sub>3</sub>), 33.8 (s, BC(CH<sub>3</sub>)<sub>3</sub>), 32.9 (s, B(Cl)C(CH<sub>3</sub>)<sub>3</sub>), 23.9 (br, BC(CH<sub>3</sub>)<sub>3</sub>), 23.3 (br, BC(CH<sub>3</sub>)<sub>3</sub>), 14.5 (d,

$P(CH_3)_3$ ,  $^1J_{PC} = 33$  Hz).  $^{11}B\{^1H\}$  NMR (128 MHz,  $C_6D_6$ ):  $\delta$  42 (s), 12 (s,  $B(Cl)(tBu)$ ).  $^{31}P\{^1H\}$  NMR (160 Hz,  $C_6D_6$ ):  $\delta$  0.5 (s). See Appendices for 2D NOESY and HMQC spectra for the assignments of **3b**. MS-ESI(+): found. 563.31736  $[M-Cl]^+$ , calcd. 563.31665.

## Preparation of 4a and 4b

Isolation of **4a**: Compound **3a** (15 mg, 0.024 mmol) and AgOTf (6.17 mg, 0.160 mmol) were dissolved in toluene (2 mL) separately. Both solutions were cooled to  $-30$  °C before being mixed. After shaking for 10 mins at room temperature, the reaction mixture was filtered through a cotton plug. The collected filtrate was then freed from volatiles to yield the crude product as a yellow solid. Recrystallization in toluene at  $-30$  °C afforded the colourless crystals of **4a** in moderate yields (estimated 30%-50%). Compound **4a** is thermally unstable, which led to decomposition over  $^{13}C\{^1H\}$  NMR and MS measurements.  $^1H$  NMR (600 MHz, toluene- $d_8$ ):  $\delta$  1.65 (s,  $NC(CH_3)_3$ , 9H), 1.57 (s,  $BC(CH_3)_3$ , 9H), 1.28 (s,  $BC(CH_3)_3OTf$ , 9H), 4.74 (m, Cy), 2.83 (m, Cy), 2.45 (m, Cy), 2.29 (m, Cy), 2.02 (m, Cy), 1.76 (m, Cy), 0.66 (d,  $^2J_{PH} = 6$  Hz,  $P(CH_3)_3$ ).  $^{11}B\{^1H\}$  NMR (128 MHz, toluene- $d_8$ ):  $\delta$  38 (s), 17 (s,  $B(OTf)(tBu)$ ).  $^{31}P\{^1H\}$  NMR (160 Hz, toluene- $d_8$ ):  $\delta$  1.17,  $^{19}F$  NMR (564 Hz, toluene- $d_8$ ):  $\delta$   $-75.9$  (s).

### Generation of 4b:

To slow down decomposition of **4b** in solution, NMR measurements were carried out at lower temperatures.  $^1H$  NMR (600 MHz, toluene- $d_8$ ,  $-28$  °C):  $\delta$  1.67 (s,  $CNC(CH_3)_3$ , 9H), 1.39 (d,  $^2J_{PH} = 12$  Hz,  $P(CH_3)_3$ ), 1.38 (s,  $NC(CH_3)_3$ , 9H), 1.14 (s,  $CBC(CH_3)_3$ , 9H), 0.77 (s,  $BC(CH_3)_3(OTf)$ , 9H).  $^{11}B\{^1H\}$  NMR (128 MHz, toluene- $d_8$ ,  $-28$  °C):  $\delta$  41.2 (s), 14.1 (s,  $B(OTf)(tBu)$ ).  $^{31}P\{^1H\}$  NMR (160 Hz, toluene- $d_8$ ,  $-28$  °C):  $\delta$  2.85,  $^{13}C\{^1H\}$  NMR (150 MHz, toluene- $d_8$ ,  $-28$  °C): 32.9 (s,  $tBu$ ), 31.4 (s,  $tBu$ ), 30.0 (s,  $tBu$ ), 29.4 (s,  $tBu$ ), 14.3 (d,  $P(CH_3)_3$ ,  $^1J_{PC} = 36$  Hz). Other signals were not observed.

## Preparation of 5a

Freshly flattened and cut lithium granules (2 mg, 0.18 mmol) were added to a DME (2 mL) solution of **3a** (50 mg, 0.08 mmol) at room temperature and the resulting reaction mixture was stirred overnight. The obtained bright orange solution was then filtered by cotton plugged pasteur pipette. The clear fluorescent orange filtrate was concentrated before being stored at  $-30$  °C to afford red crystals of **5a**. (28 mg, 0.041 mmol, 51%).  $^1H$  NMR (500 MHz,  $C_6D_6$ ):  $\delta$  1.91 ( $NC(CH_3)_3$  and  $BC(CH_3)_3$ , s, 18H), 1.56 ( $BC(CH_3)_3$ , s, 9H), 0.99 (d,  $^2J_{PH} = 6$  Hz,  $P(CH_3)_3$ , 9H);  $^{13}C\{^1H\}$  NMR (126 MHz,  $C_6D_6$ ):  $\delta$  140.5 (br, d, AuC), 70.5 (s, br, OCH<sub>3</sub>), 59.0 (s, OCH<sub>2</sub>), 56.7 (s, NCH (Cy)), 52.1 ( $NC(CH_3)_3$ ), 39.0 (s,  $NC(CH_3)_3$ ), 35.8 (s,  $BC(CH_3)_3$ ), 33.4 (s,  $BC(CH_3)_3$ ), 33.9 (s, CH<sub>2</sub> (Cy)), 32.0 (s, CH<sub>2</sub> (Cy)), 27.5 (s, CH<sub>2</sub> (Cy)), 27.2 (s, CH<sub>2</sub> (Cy)), 26.6 (s, CH<sub>2</sub> (Cy)), 22.5 (br,  $BC(CH_3)_3$ ), 22.0 (br,  $BC(CH_3)_3$ ), 16.60 (d,  $P(CH_3)_3$ ,  $^2J_{PC} = 25$  Hz).  $^{11}B\{^1H\}$  NMR (160 MHz,  $C_6D_6$ ):  $\delta$  42.0 (s), 34.0 (s).  $^{31}P\{^1H\}$  NMR (202 MHz,  $C_6D_6$ ):  $\delta$  6.5 (s).  $Li\{^1H\}$  NMR (194 MHz,  $C_6D_6$ ):  $\delta$  1.3 ppm. MS-ESI(+):  $m/z$  found 607.34656  $[M-PMe_3+H_2O]^+$ , calcd. 607.34365.

## Crystallographic Studies (3a/b, 4a and 5a)

### General Considerations

Crystals suitable for the X-ray structural determination were mounted on a Bruker SMART APEXII CCD diffractometer and irradiated with graphite monochromated Mo  $K\alpha$  radiation ( $\lambda = 0.71073$  Å) for data collection. The data were processed using the APEX3 program suite. All structures were solved by an intrinsic phasing method using the SHELXT program (ver. 2014/4–2014/5)<sup>S3</sup>. Refinement on  $F^2$  was carried out using full-matrix least-squares with the SHELXL<sup>S4</sup> and expanded using Fourier techniques. All nonhydrogen atoms, except those of disordered solvents, were refined using anisotropic thermal parameters. Hydrogen atoms were assigned to idealized geometric positions and included in structure factor calculations. The SHELX was interfaced with SHELXLE GUI for most of the refinement steps<sup>S5</sup>. The pictures of the molecules were prepared using Pov-Ray 3.6<sup>S6</sup>.

Table 1. Crystal data for 3a-5a.

Crystal data	(3a)	(3b)	(4a)	(5a)
CCDC numbers	2109025	2109026	2109027	2109028
Chemical formula	C <sub>22</sub> H <sub>47</sub> AuB <sub>2</sub> ClN <sub>2</sub> P	C <sub>10</sub> H <sub>22.50</sub> Au <sub>0.50</sub> BCl <sub>0.50</sub> NP <sub>0.50</sub>	C <sub>26.50</sub> H <sub>51</sub> AuB <sub>2</sub> F <sub>3</sub> N <sub>2</sub> O <sub>3</sub> PS	C <sub>26</sub> H <sub>57</sub> AuB <sub>2</sub> LiN <sub>2</sub> O <sub>2</sub> P
<i>M<sub>r</sub></i>	624.62	598.58	784.31	686.23
Crystal system, space group	Triclinic, <i>P</i> −1	Triclinic, <i>P</i> −1	Triclinic, <i>P</i> −1	Monoclinic, <i>P</i> <sub>2</sub> / <i>n</i>
Temperature (K)	100(2)	173(2)	173(2)	173(2)
Wavelength	0.71073 Å	0.71073 Å	0.71073 Å	0.71073 Å
<i>a</i> , <i>b</i> , <i>c</i> (Å)	10.294 (8), 11.66 (1), 12.419 (11)	10.461 (5), 10.965 (6), 12.083 (6)	10.469 (7), 11.938 (8), 14.578 (10)	11.464 (10), 18.202 (18), 16.405 (16)
$\alpha$ , $\beta$ , $\gamma$ (°)	84.959 (17), 68.147 (7), 87.188 (14)	83.701 (7), 89.220 (8), 75.206 (6)	83.771 (14), 81.751 (5), 72.088 (15)	90, 103.720 (5), 90
<i>V</i> (Å <sup>3</sup> )	1378 (2)	1331.8 (12)	1712 (2)	3326 (5)
<i>Z</i>	2	2	2	6
Radiation type	Mo <i>K</i> $\alpha$	Mo <i>K</i> $\alpha$	Mo <i>K</i> $\alpha$	Mo <i>K</i> $\alpha$
Absorption coefficient $\mu$ (mm <sup>−1</sup> )	5.5	5.69	4.45	4.49
Crystal size (mm)	0.18 × 0.08 × 0.07	0.04 × 0.04 × 0.03	0.29 × 0.25 × 0.19	0.09 × 0.07 × 0.04
Data collection				
Diffractometer	Bruker APEX-II CCD	Bruker APEX-II CCD	Bruker APEX-II CCD	Bruker APEX-II CCD
Absorption correction	–	–	Multi-scan	Multi-scan
<i>T</i> <sub>min</sub> , <i>T</i> <sub>max</sub>	–	–	0.356, 0.488	0.613, 0.851
No. of measured, independent and observed [ <i>I</i> > 2 $\sigma$ ( <i>I</i> )] reflections	13420, 4858, 4703	5434, 3619, 2380	20414, 8110, 7336	39338, 7937, 6036
<i>R</i> <sub>int</sub>	0.023	0.085	0.021	0.057
$\theta$ <sub>max</sub> (°)	25	23.3	28	28
( <i>sin</i> $\theta$ / $\lambda$ ) <sub>max</sub> (Å <sup>−1</sup> )	0.595	0.555	0.661	0.661
<i>R</i> [ <i>F</i> <sup>2</sup> > 2 $\sigma$ ( <i>F</i> <sup>2</sup> )], <i>wR</i> ( <i>F</i> <sup>2</sup> ), <i>S</i>	0.016, 0.039, 1.09	0.064, 0.139, 0.95	0.022, 0.051, 1.04	0.030, 0.059, 1.01
No. of reflections	4858	3619	8110	7937
No. of parameters	274	247	401	330
No. of restraints	0	0	57	0
H-atom treatment	H-atom parameters constrained	H-atom parameters constrained	H-atom parameters constrained	H-atom parameters constrained
$\Delta\rho$ <sub>max</sub> , $\Delta\rho$ <sub>min</sub> (e Å <sup>−3</sup> )	0.76, −0.30	2.46, −2.00	1.63, −0.53	0.74, −0.44

## Computational Details

All the Density Functional Theory (DFT) calculations were done using Gaussian 09 rev E.01 software package.<sup>S7</sup> First, we performed gas-phase geometry optimizations with the  $\omega$ B97X-D<sup>S8</sup> density-functional in combination with a mixed triple- $\zeta$  quality basis sets: LANL2TZ(f) for Au atom,<sup>S9</sup> People's 6-311G(2d) for P and S atoms (with two polarization functions) and 6-311G(d) for the remaining atoms. A subsequent harmonic frequency calculation, for each optimized geometry, was executed to corroborate the character of each critical point in the potential energy surface (PES): reactants, intermediates and products must present all the frequencies as positive whereas transition state must have one and just one negative frequency. Thermal and entropy corrections to the total energy were taken from the thermochemistry analysis in the output file at 298K and 1 atm.

Also, we performed calculations for including the solvent effect through the PCM model<sup>S10</sup> using the SMD parameters<sup>S11</sup> according to the Truhlar's model using benzene as solvent. These calculations were performed as single points of the optimized geometry. The obtained energies were added to the gas-phase calculations reported as our final values.

Moreover, we utilized the NBO7.0 program<sup>S12</sup> for analyzing the bonding mechanism of the chemical structures obtained, and the IBO program<sup>S13</sup> for plotting the intrinsic bond orbitals.

## Selected Kohn-Sham Molecular Orbitals of BNC-1, CAAC and NHC

### Molecular Orbitals of BNC-1

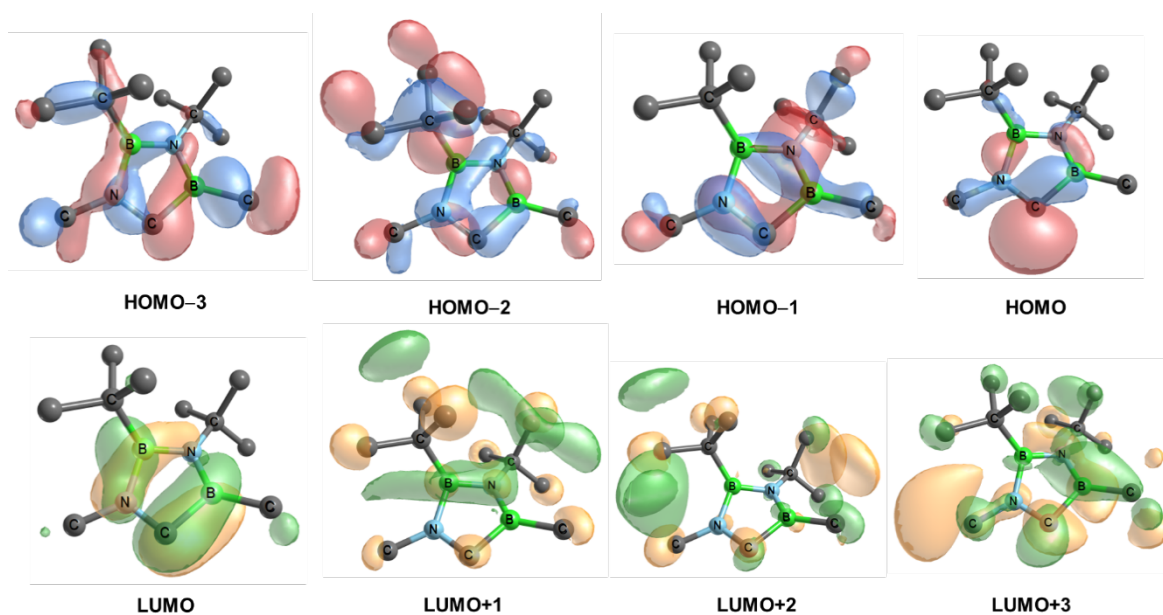


Figure S1. Molecular Orbitals of BNC-1 (isosurface = 0.04 a.u.)

## Frontier Molecular Orbitals of 3a-5a

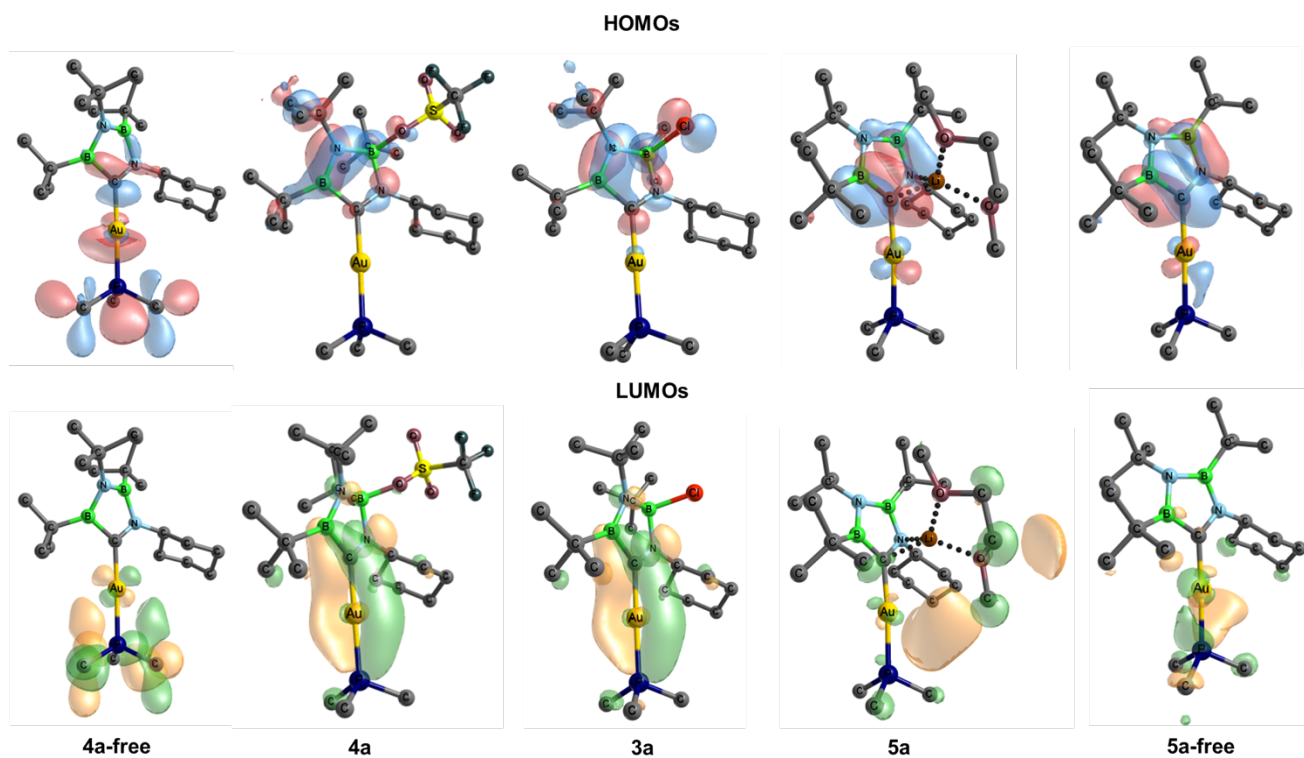


Figure S2. Frontier Molecular orbitals of 4a-free, 4a, 3a, 5a, and 5a-free (isosurface = 0.04 a.u.).

## Molecular Orbitals of BNC, CAAC and NHC carbenes

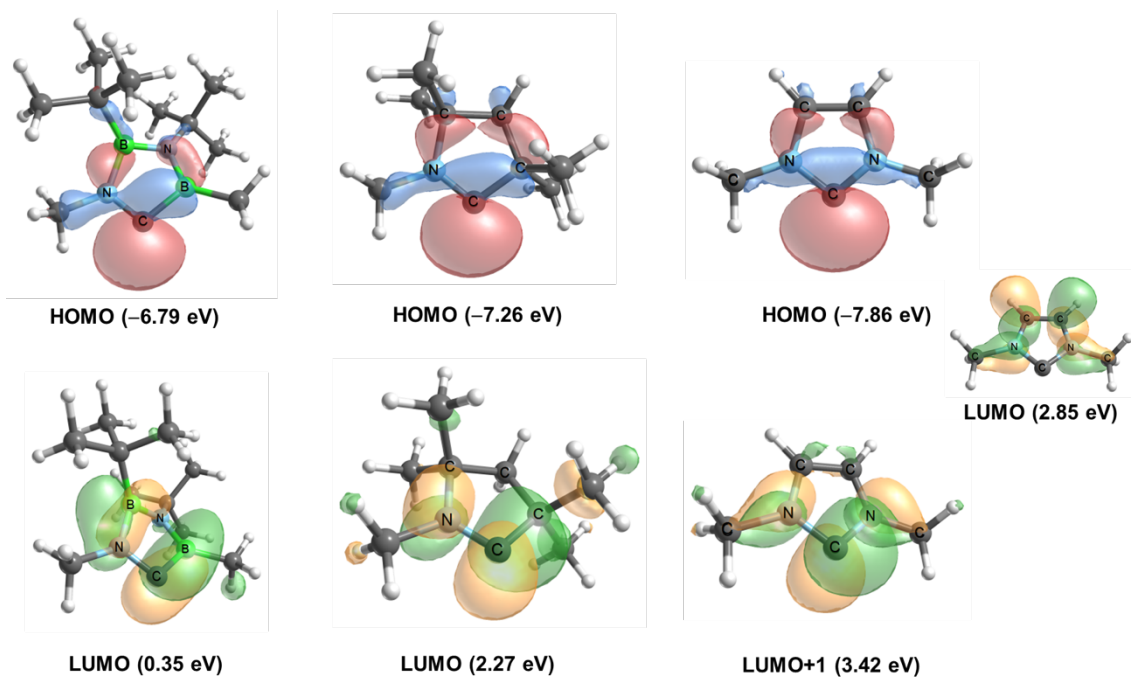
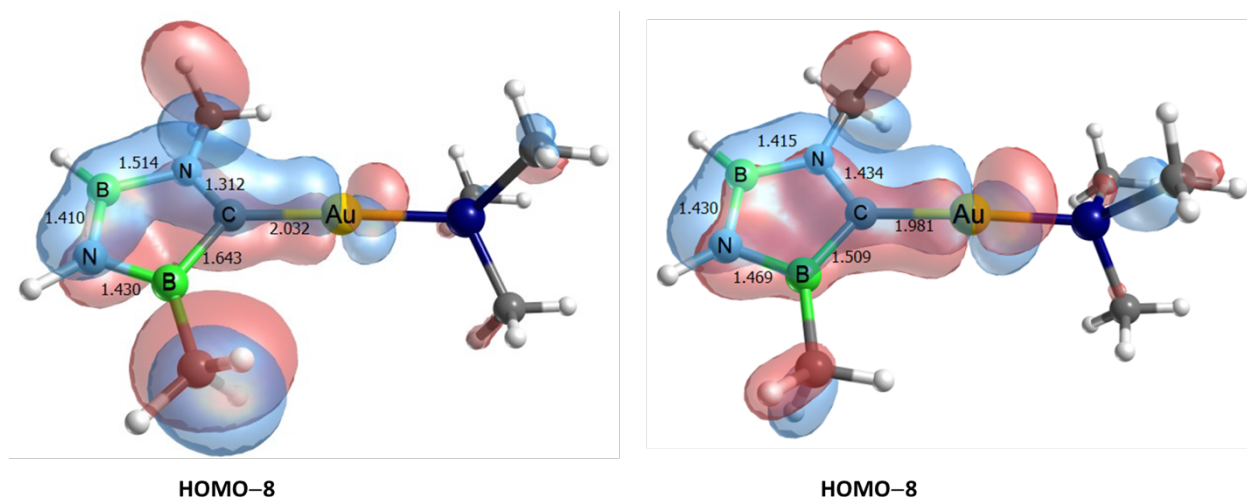


Figure S3. Molecular orbitals that correlate with the  $E_\sigma$  (HOMOs) and  $E_\pi^*$  (LUMOs) (isosurface = 0.04 a.u.) of BNC-1, CAAC, and NHC.

## Relevant Molecular Orbitals of the simplified BNC gold complexes



**Figure S4.** Molecular Orbitals showing the  $\pi$ -backdonation for the simplified cationic **BNC-AuPMe<sub>3</sub>** (left) and anionic **(BNC-2)-AuPMe<sub>3</sub>** (right) gold complexes (isosurface = 0.04 a.u.) Bond distances are giving in angstroms (Å).

### HOMO-LUMO gap of BNC-1 and BNC-1-OTF

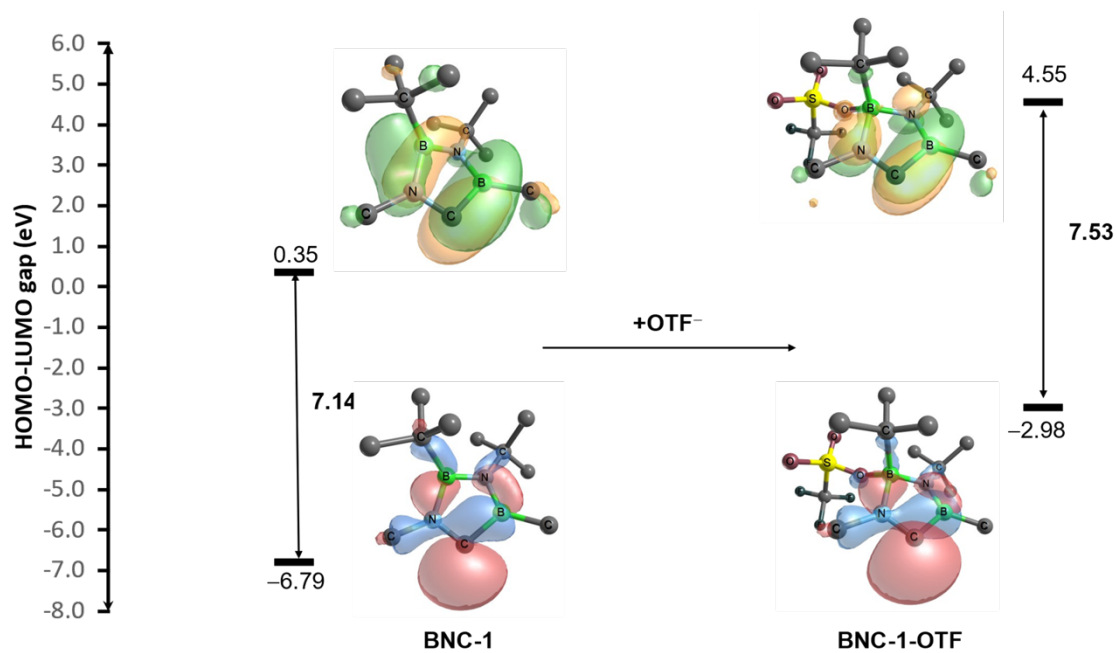


Figure S5. HOMO-LUMO gap of BNC-1 and BNC-1-OTF.

### Fluclional process of 4a

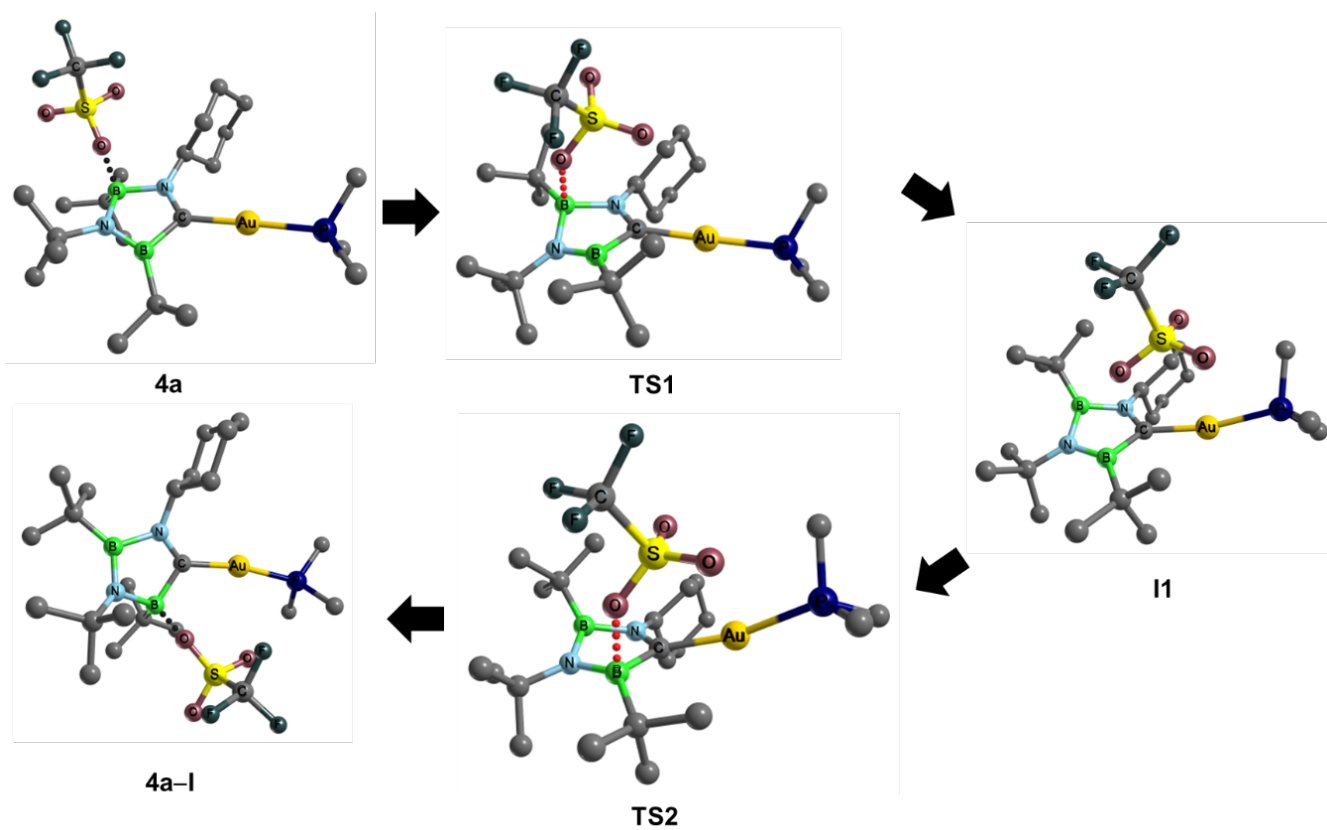


Figure S6. Optimized geometries of each reaction step of the proposed fluclional process.



## Natural Bond Orbital (NBO) Analysis

The second order perturbative energies of NBO<sup>S15</sup>,  $E(2)$ , were analyzed to compare the  $\pi$ -accepting properties of a BNC carbene amongst simple CAAC and NHC carbenes. For this, only the most important donor-acceptor interaction energy between a  $d$  gold orbital and the  $\pi^*(\text{N-C})$  of the heterocyclic ring was considered,  $E_{\text{Au} \rightarrow \text{C}}$  (Figure S6). In Table S2 these values are given in decreasing order of  $\pi$ -accepting ability of each ring. Noteworthy, the introduction of a  $\pi$ -acceptor ligand, such as  $\text{PMe}_3$ , decreases the  $E_{\text{Au} \rightarrow \text{C}}$ .

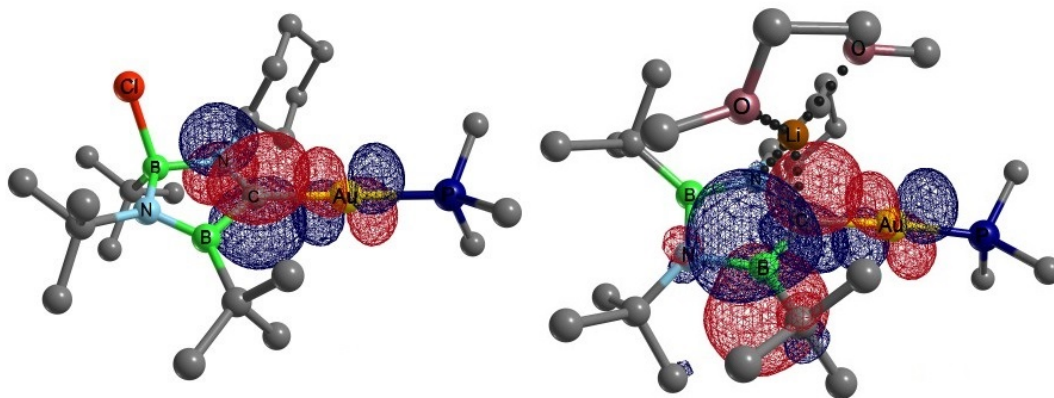


Figure S7. NBO Donor-acceptor plot between NBOs  $d(\text{Au}) \rightarrow \pi^*(\text{N-C})$  of complex **4a** (left) and  $d(\text{Au}) \rightarrow \pi^*(\text{C-B})$  of **5a** (right).

For complexes shown in Table S3, we used NBO version 3.1<sup>S14</sup> as implemented in gaussian 09 rev. E.01 only to quantify the donor acceptor interaction between the carbon lone pair of electrons and the vacant  $6p$  orbital of gold (Figure S7).

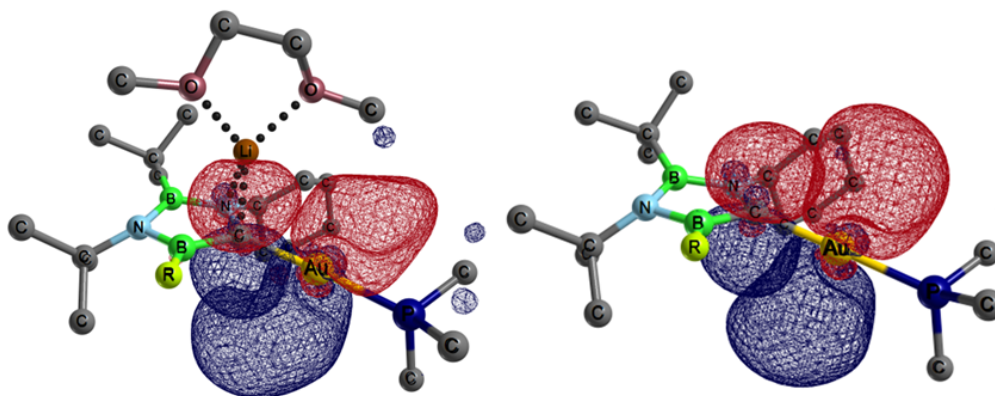


Figure S8. NBO Donor-acceptor plot between NBOs  $p(\text{C}) \rightarrow p(\text{Au})$  of complex **5a** (left) and **5a-free** (right) ( $\text{R} = t\text{Bu}$ ).

**Table S2.** Donor-acceptor interaction energies (kcal/mol) of  $d(\text{Au}) \rightarrow \pi^*(\text{N}-\text{C})$  ( $E_{\text{Au} \rightarrow \text{C}}$ ). NBO charges and Wiberg bond index shown as red and blue numbers, respectively.

	Structure	$E_{\text{Au} \rightarrow \text{C}}$
BNC-AuCl		30.5
CAAC-AuCl		25.4
NHC-AuCl		22.6
$[(\text{Ph})_2\text{C}-\text{Au}-\text{PMe}_3]^+$		25.0 <sup>(A)</sup>
BNC-AuPMe <sub>3</sub>		16.9
4-free		13.9
4a		10.6
3a		10.0

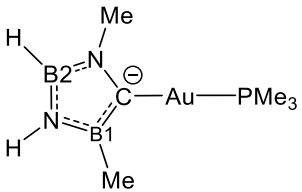
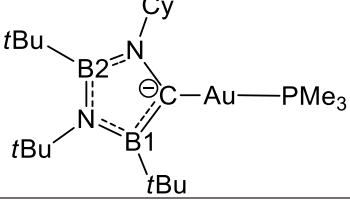
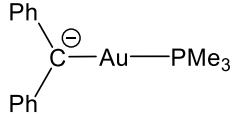
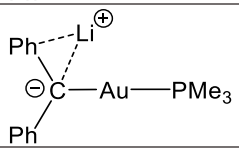
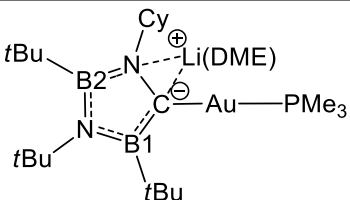
Li[(Ph) <sub>2</sub> C-Au-PMe <sub>3</sub> ]		4.6 <sup>[B]</sup>
[(Ph) <sub>2</sub> C-Au-PMe <sub>3</sub> ] <sup>-</sup>		4.2 <sup>[B]</sup>
5a-free <sup>[A]</sup>		3.3 <sup>[C]</sup>
5a <sup>[A]</sup>		3.1 <sup>[C]</sup>
(BNC <sup>-2</sup> )-AuPMe <sub>3</sub>		2.9 <sup>[C]</sup>
(Ph) <sub>2</sub> C(OTF)-Au-PMe <sub>3</sub>		--

[A] Donor-acceptor interaction energy,  $E_{Au \rightarrow C}$ , calculated between  $d(Au) \rightarrow p(C)$  NBOs.

[B] Donor-acceptor interaction energy,  $E_{Au \rightarrow C}$ , calculated between  $d(Au) \rightarrow \pi^*(C-C)$  NBOs.

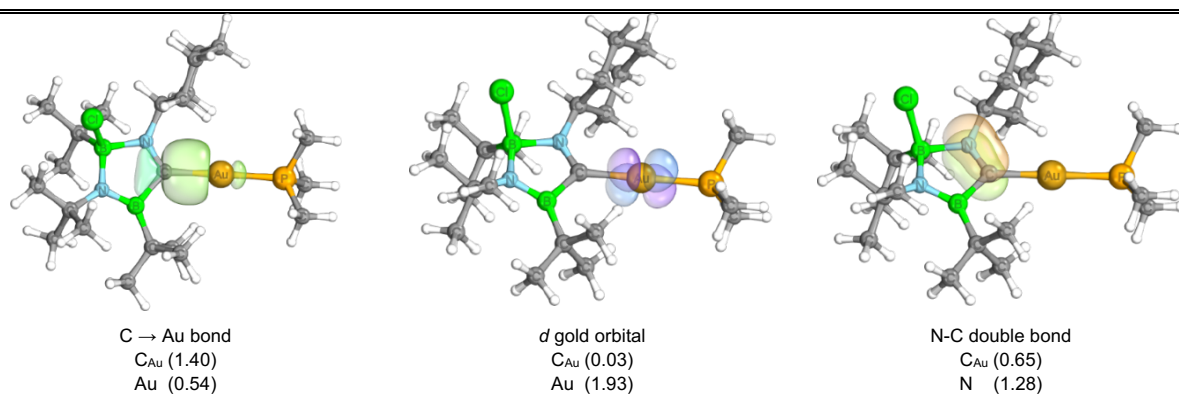
[C] Donor-acceptor interaction energy,  $E_{Au \rightarrow C}$ , calculated between  $d(Au) \rightarrow \pi^*(C-B)$  NBOs.

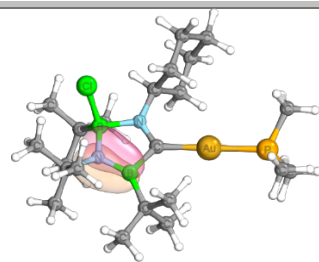
**Table S3.** Donor-acceptor interaction energies (kcal/mol) of p(C)→p(Au) ( $E_{p(C) \rightarrow p(Au)}$ ). Values were calculated with NBO v. 3.1.

Structure	$E_{p(C) \rightarrow p(Au)}$
 (BNC-2)-AuPMe <sub>3</sub>	70.1
 5a-free	42.5
 (Ph) <sub>2</sub> C-Au-PMe <sub>3</sub>	37.7
 Li[(Ph) <sub>2</sub> C-Au-PMe <sub>3</sub> ]	18.3
 5a	15.5

## Intrinsic Bond Orbitals (IBO)

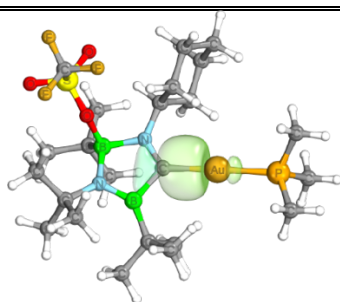
IBO method connects the quantitative self-consistent field wave functions to a qualitative chemical picture, such as the nature and shape of chemical bonds, without any empirical input. Selected Intrinsic Bond Orbitals (IBOs) are shown below of complexes **3a-5a**, along with the fractions of electrons in parentheses of each atom involved in the doubly occupied orbital.



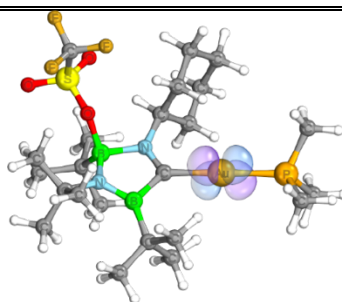


N-B double bond  
 B (0.42)  
 N (1.46)

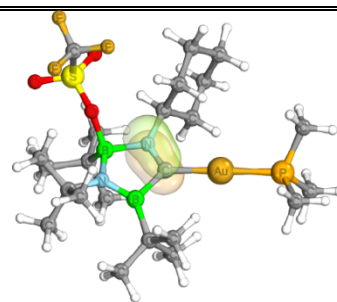
Figure S9. Most important Intrinsic Bond Orbitals of compound 3a.



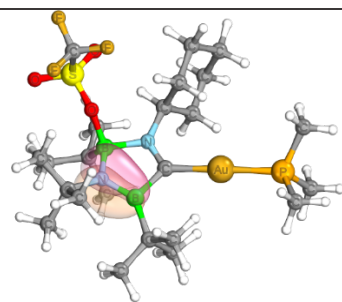
C → Au bond  
 C<sub>Au</sub> (1.41)  
 Au (0.54)



*d* gold orbital  
 C<sub>Au</sub> (0.03)  
 Au (1.93)

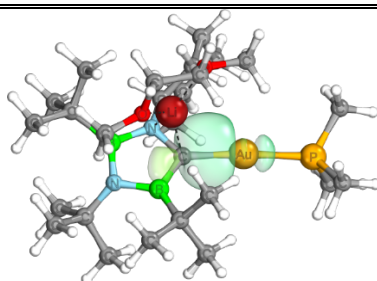


N-C double bond  
 C<sub>Au</sub> (0.64)  
 N (1.29)

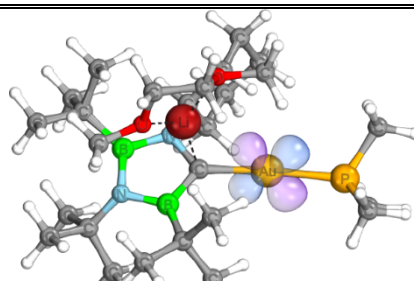


N-B double bond  
 B (0.38)  
 N (1.49)

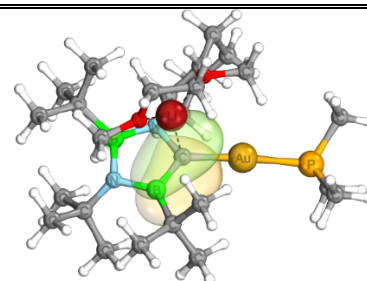
Figure S10. Most important Intrinsic Bond Orbitals of compound 4a.



C → Au bond  
 C<sub>Au</sub> (1.31)  
 Au (0.61)



*d* gold orbital  
 P (0.04)  
 Au (1.94)



C-B double bond  
 C<sub>Au</sub> (1.34)  
 B (0.50)  
 Li (0.03)

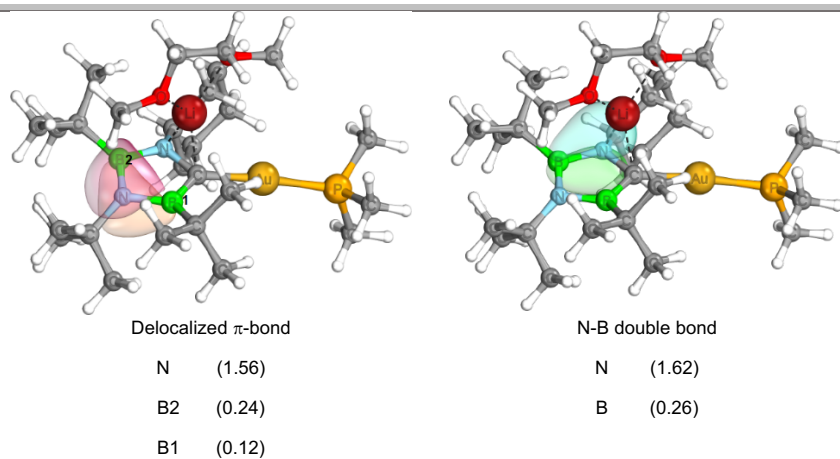


Figure S11. Most important Intrinsic Bond Orbitals of compound 5a.

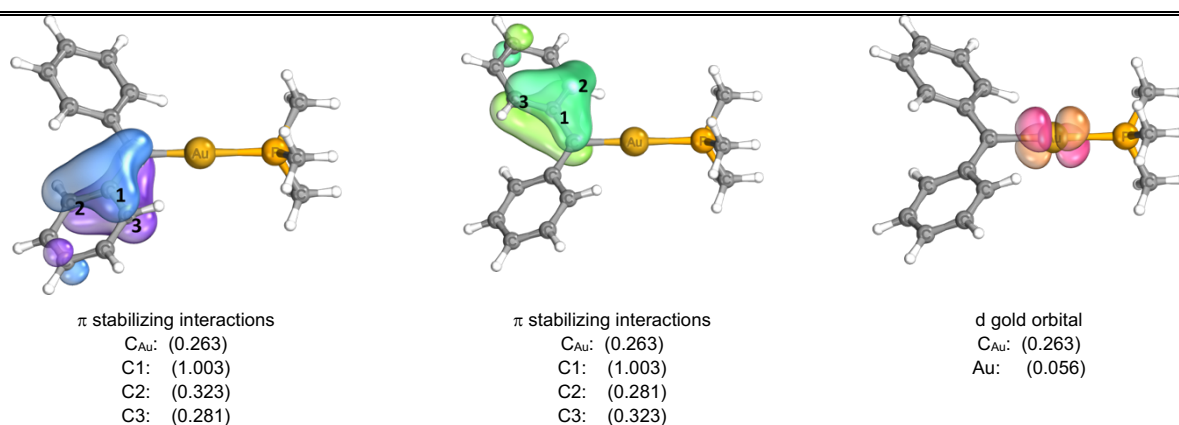


Figure S12. Most important Intrinsic Bond Orbitals of cationic compound 6-free.

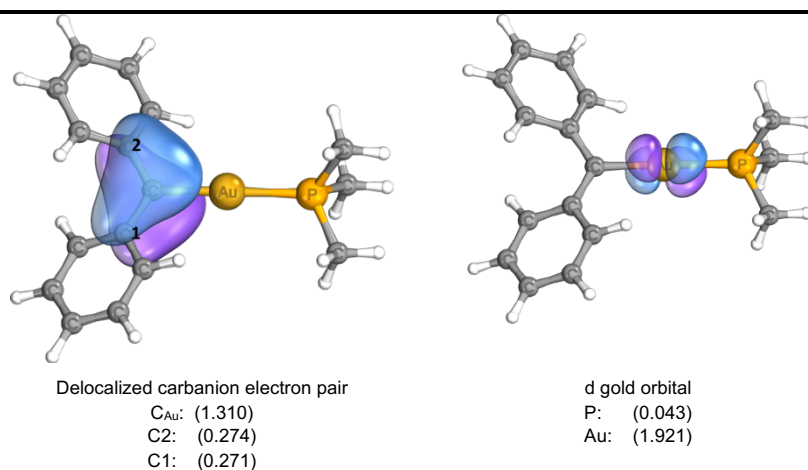


Figure S13. Most important Intrinsic Bond Orbitals of anionic compound 7-free.

## NCI and AIM analysis of 5a

To corroborate the presence of a carbanion in **5a**, a comparison between the Theory of Atoms in Molecules (AIM)<sup>S16</sup> and Non-Covalent Interactions (NCI)<sup>S17</sup> calculations for **5a** and the simple system **5NC** were performed. Compound **5NC** (Figure S11) contains a carbanion and a nitrogen lone pair, both interacting with the Li(DME), simulating the N-C bonding of the BNC ring from **5a**. The obtained results are similar, except that in **5a** these lone pairs are delocalized towards the boron atoms and, thus, validates the presence of a carbanion in **5a**.

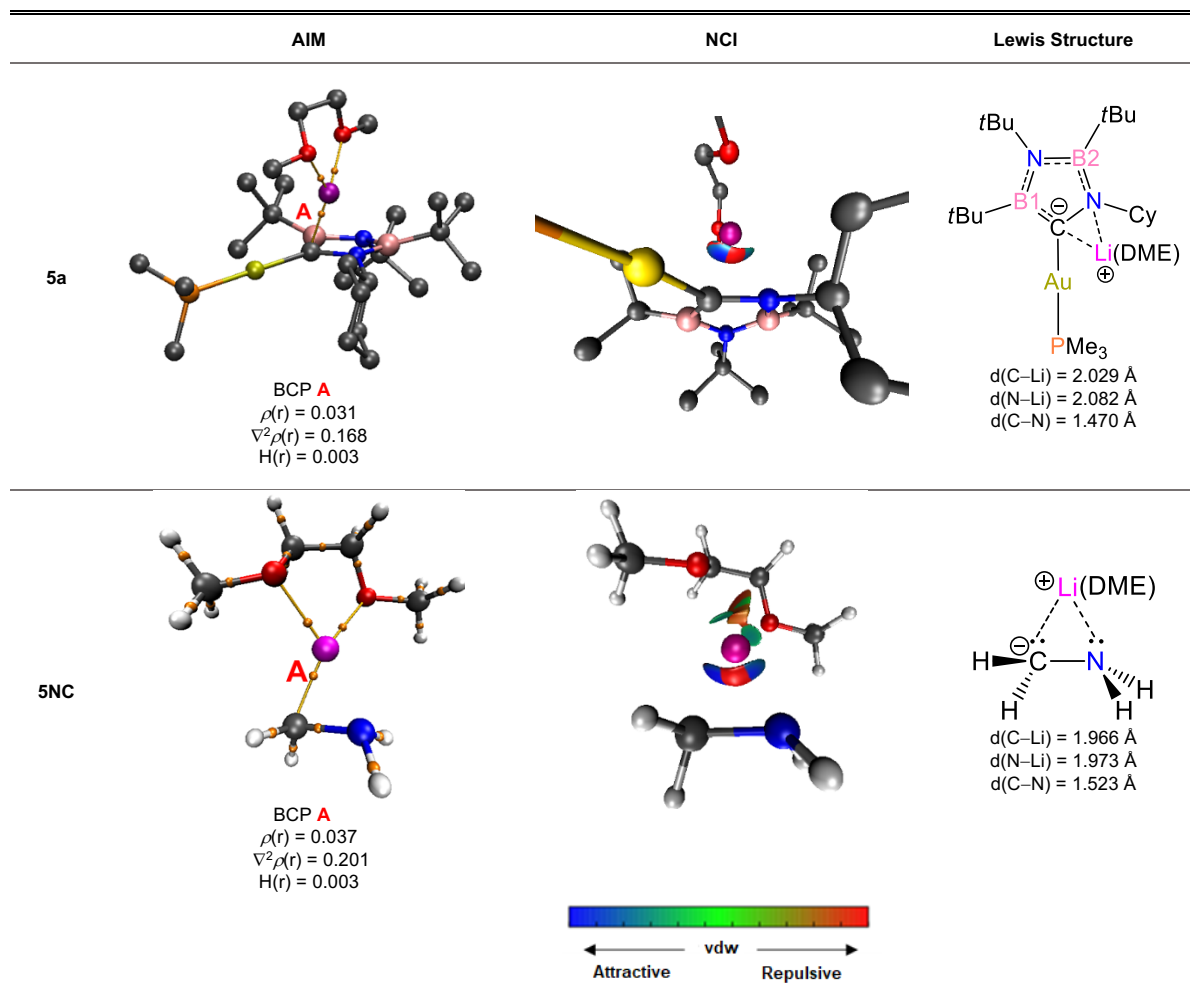


Figure S14. AIM and NCI results of **5a** and **5NC**, along with the C-Li and N-Li distances.

## Nucleus Independent Chemical Shift (NICS)

The Nucleus Independent Chemical Shift (NICS) is a method that measures the induced electromagnetic field in a point for a cyclic system. This can be used to determine aromatic, antiaromatic and non-aromatic systems that have negative, positive and both values respectively, along the distance perpendicular to the ring plane. For complexes **4a**, **4a-I**, **I1** and **5a**, the NICS values were calculated in the direction perpendicular to the BNC ring in the side that does not contains a nearby substituent that can affect these values.

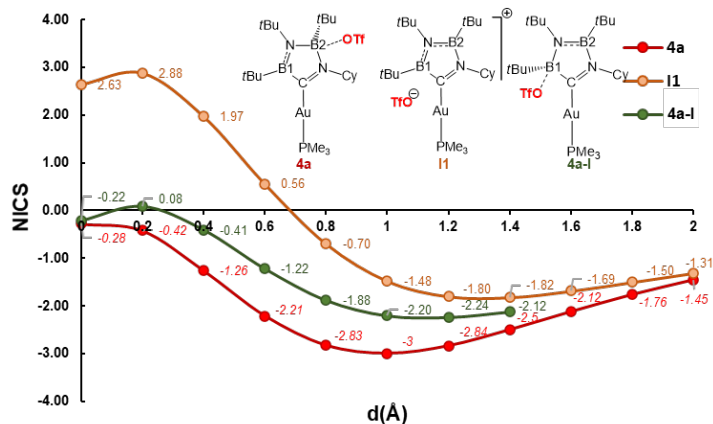


Figure S15. NICS profile of the complexes involved in the fluxional process for **4a**.

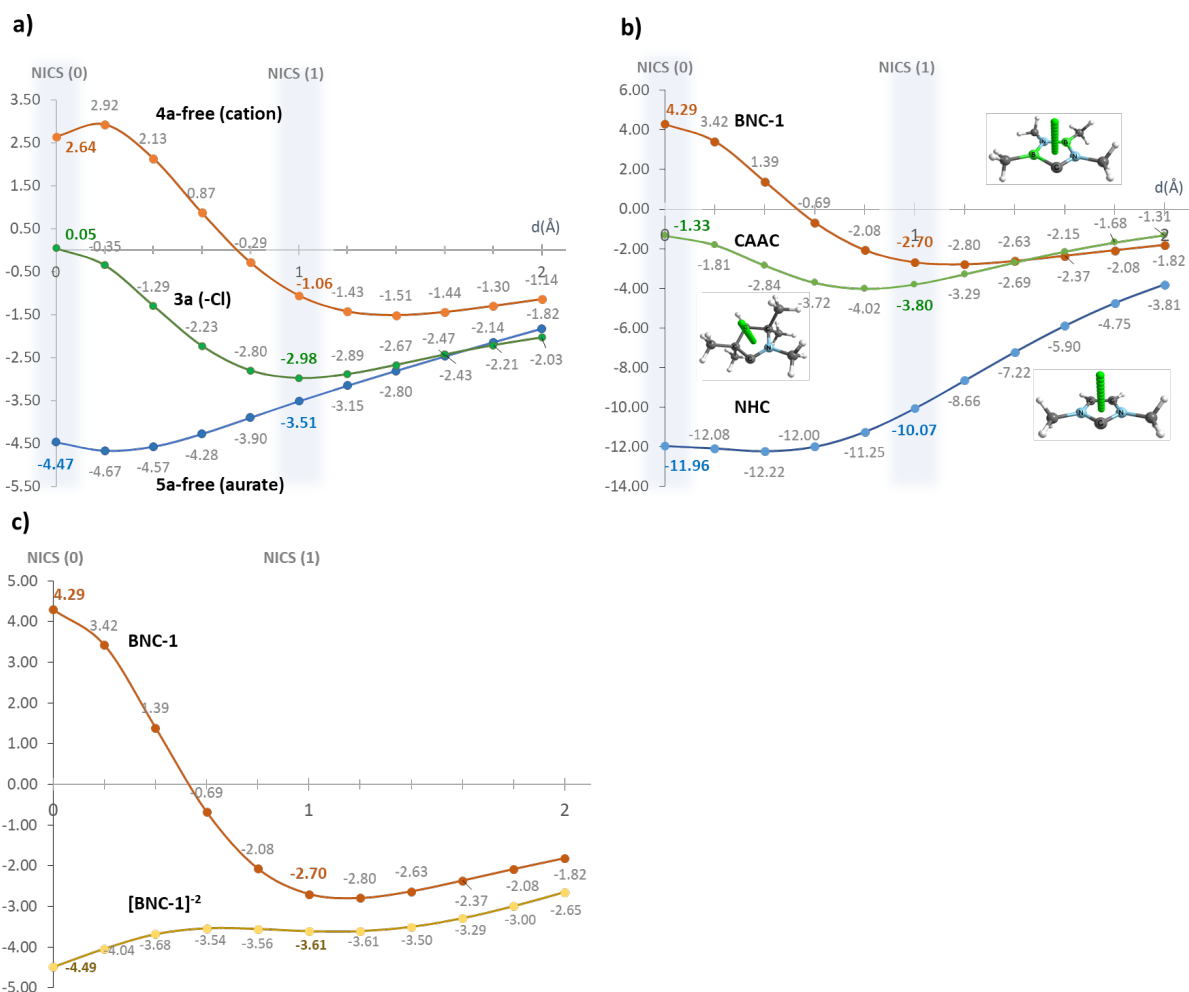


Figure S16. NICS profiles of a) **4a-free**, **3a**, **5a-free**, b) metal free ligands **BNC-1** (1,2,3,4-tetramethyl-5 $\lambda^2$ -1,3,2,4-diazadiborolidine), **CAAC** and **NHC** and c) comparison between **BNC-1** and its dianionic form **[BNC-1]<sup>2-</sup>**.



## Proposed Reaction Mechanism of 2 with CN*t*Bu

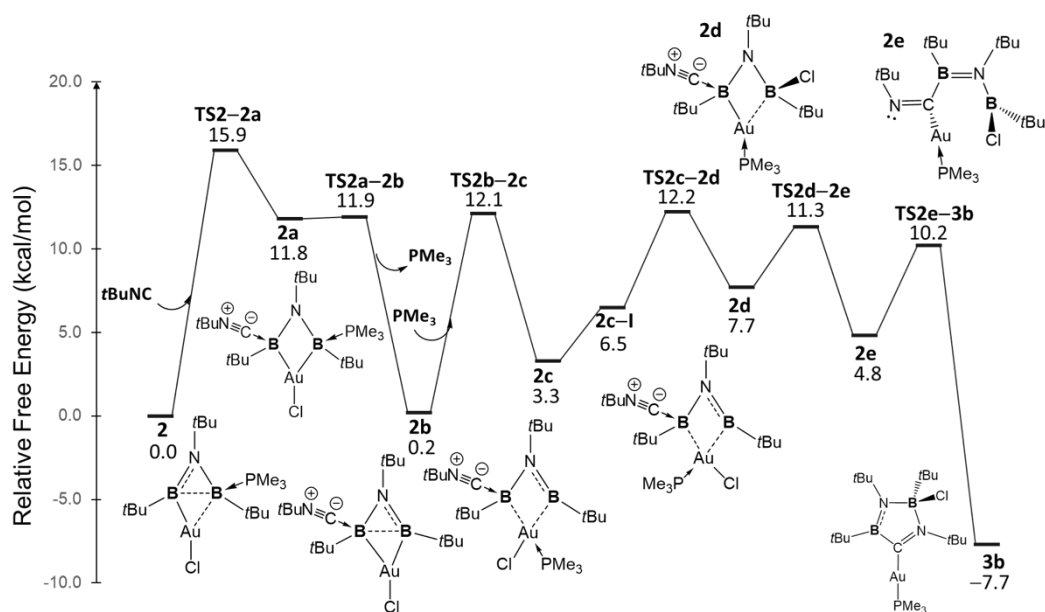


Figure S17. Plausible reaction mechanism of 2 with CN*t*Bu calculated at (SMD: Benzene)<sub>ω</sub>B97X-D/[Au: LANL2TZ(f), P: 6-311g(2d), rest: 6-311g(d)].

## Calculated $^{11}\text{B}\{^1\text{H}\}$ and $^{13}\text{C}\{^1\text{H}\}$ NMR of 3a and 5a

Table S4. Calculated  $^{11}\text{B}$  and  $^{13}\text{C}$  NMR for relevant atoms of 3a and 5a. Methodology of reference S18 was used to perform these calculations.

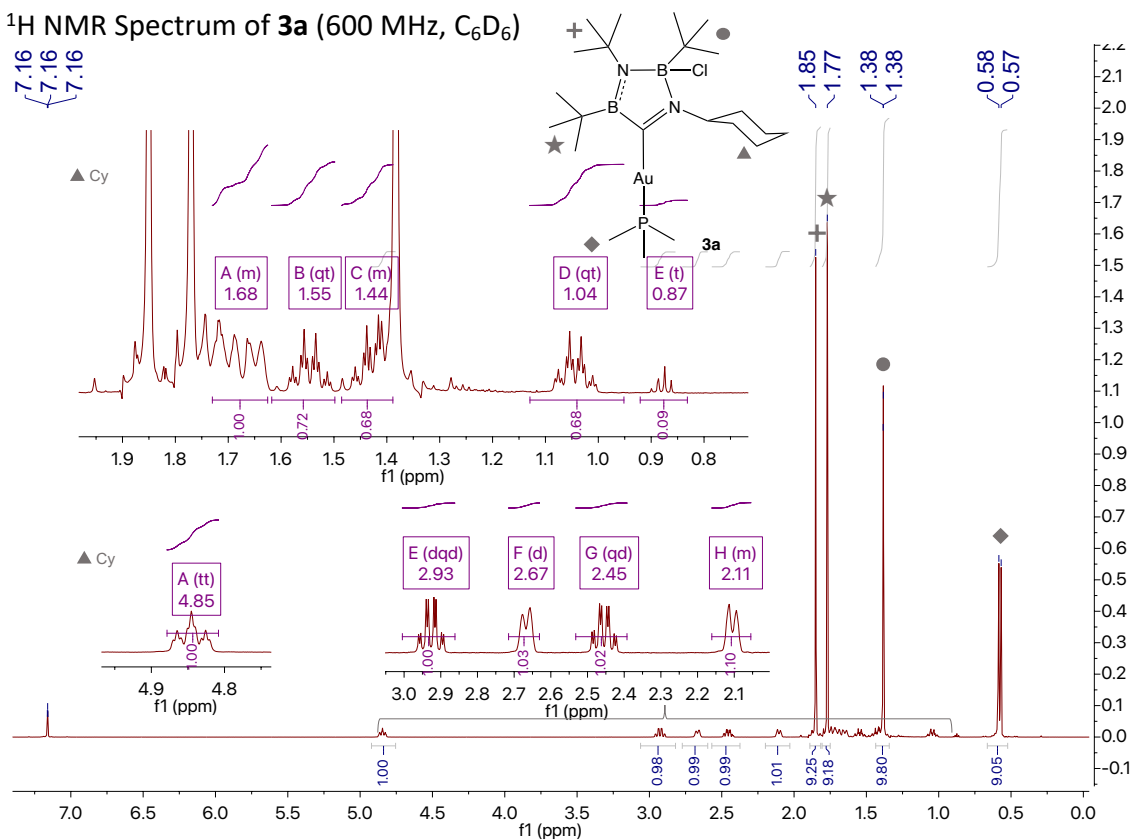
	NMR (ppm)		
	Atom	Experimental	Calculated <sup>[A]</sup>
<p><b>3a</b></p>	B1	41.9	41.9
	B2	12.0	10.6
	C1	251.3	247.2
<p><b>5a</b></p>	B1	41.9	41.9
	B2	33.9	34.0
	C1	140.5	128.0

## References

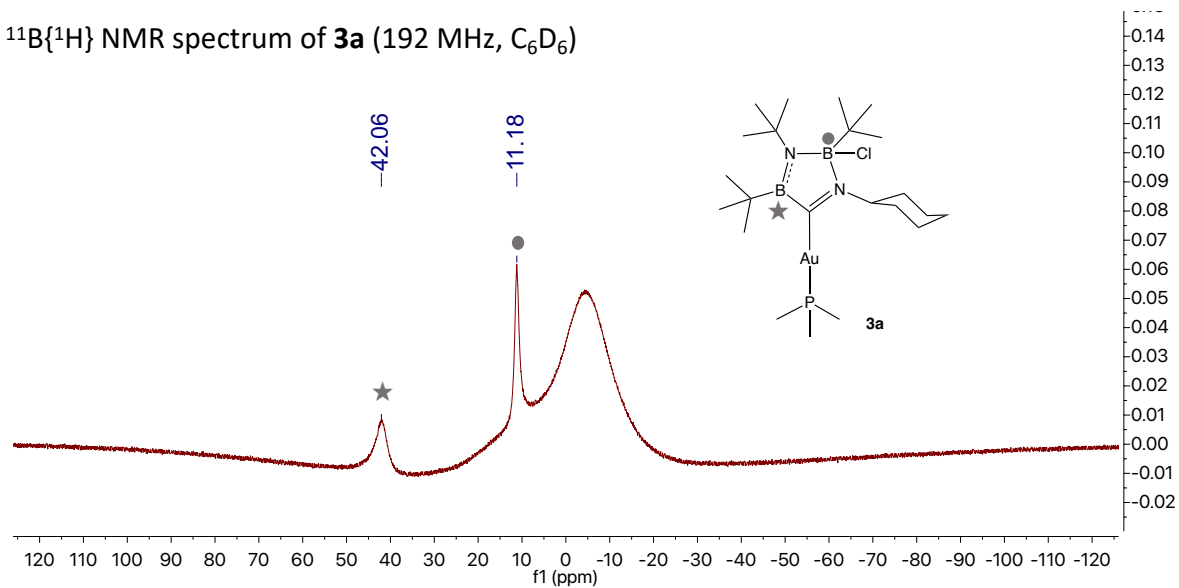
- [S1] a) K. H. Van Bonn, P. Schreyer, P. Paetzold, R. Boese, *Chem. Ber.* **1988**, *121*, 1045-1057. b) R. Boese, B. Kroeckert, P. Paetzold, *Chem. Ber.* **1987**, *120*, 1913-1915.
- [S2] R. Shang, S. Saito, J. O. C. Jimenez-Halla, Y. Yamamoto, *Dalton Trans.* **2018**, *47*, 5181-5188.
- [S3] G. Sheldrick, *Acta Crystallogr., Sect. A: Found. Adv.*, **2015**, *71*, 3–8.
- [S4] G. M. Sheldrick, *Acta Crystallogr., Sect. A: Found. Crystallogr.*, **2008**, *A64*, 112–122.
- [S5] C. B. Huebschle, G. M. Sheldrick and B. Dittrich, *J. Appl. Crystallogr.*, **2011**, *44*, 1281–1284.
- [S6] C. Cason, *Pov-Ray 3.6.2 Persistence of Vision, Raytracer*, **2009**.
- [S7] Gaussian 09, Revision E.01, Frisch, M. J., Trucks, G. W., Schlegel, H. B., Scuseria, G. E., Robb, M. A., Cheeseman, J. R., Scalmani, G., Barone, V., Mennucci, B., Petersson, G. A., Nakatsuji, H., Caricato, M., Li, X., Hratchian, H. P., Izmaylov, A. F., Bloino, J., Zheng, G., Sonnenberg, J. L., Hada, M., Ehara, M., Toyota, K., Fukuda, R., Hasegawa, J., Ishida, M., Nakajima, T., Honda, Y., Kitao, O., Nakai, H., Vreven, T., Montgomery, J. A., Jr., Peralta, J. E., Ogliaro, F., Bearpark, M., Heyd, J. J., Brothers, E., Kudin, K. N., Staroverov, V. N., Kobayashi, R., Normand, J., Raghavachari, K., Rendell, A., Burant, J. C., Iyengar, S. S., Tomasi, J., Cossi, M., Rega, N., Millam, J. M., Klene, M., Knox, J. E., Cross, J. B., Bakken, V., Adamo, C., Jaramillo, J., Gomperts, R., Stratmann, R. E., Yazyev, O., Austin, A. J., Cammi, R., Pomelli, C., Ochterski, J. W., Martin, R. L., Morokuma, K., Zakrzewski, V. G., Voth, G. A., Salvador, P., Dannenberg, J. J., Dapprich, S., Daniels, A. D., Farkas, Ö., Foresman, J. B., Orti.
- [S8] J.-D. Chai, M. Head-Gordon, *Phys. Chem. Chem. Phys.* **2008**, *10*, 6615-6620.
- [S9] a) Hay, P.J. and Wadt, W.R. *J. Chem. Phys.* **1985**, *82*, 299. b) Roy, L.E.; Hay, P.J. and Martin, R.L. *J. Chem. Theory Comput.* **2008**, *4*, 1029. c) Ehlers, A.W.; Bohme, M.; Dapprich, S.; Gobbi, A.; Hollwarth, A.; Jonas V.; Kohler, K.F.; Stegmann, R.; Veldkamp, A.; Frenking, G. *Chem. Phys. Lett.* **1993**, *208*, 111.
- [S10] a) Barone, V. and Cossi, M. *J. Phys. Chem. A* **1998**, *102*, 1995. b) Cossi, M.; Barone, V.; Mennucci, B. and Tomasi, J. *Chem. Phys. Lett.* **1998**, *286*, 253. c) Barone, V.; Cossi, M. and Tomasi, J. *J. Comp. Chem.* **1998**, *19*, 404. d) Tomasi, J.; Mennucci, B. and Cammi, R. *Chem. Rev.* **2005**, *105*, 2999.
- [S11] Marenich, A. V.; Cramer, C. J. and Truhlar, D. G. *J. Phys. Chem. B* **2009**, *113*, 6378.
- [S12] E. D. Glendening, J. K. Badenhoop, A. E. Reed, J. E. Carpenter, J. A. Bohmann, C. M. Morales, P. Karafiloglou, C. R. Landis, and F. Weinhold, Theoretical Chemistry Institute, University of Wisconsin, Madison, WI, **2018**, *NBO 7.0*.
- [S13] a) Knizia, G. *J. Chem. Theory Comput.* **2013**, *9*, 4834. b) Knizia, G. J.E.M.N. Klein, *Angew. Chem. Int. Ed.* **2015**, *54*, 5518.
- [S14] Glendening, E. D.; Reed, A. E.; Carpenter J. E. and Weinhold. F. *NBO Version 3.1*.
- [S15] Reed, A. E., Curtiss, L. A., Weinhold, F. *Chem. Rev.* **1988**, *88*, 899–926.
- [S16] R. F. W. Bader, Oxford University Press, Oxford, **1990**.
- [S17] E.R. Johnson, S. Keinan, P. Mori-Sánchez, J. Contreras-García, A. J. Cohen, W. Yang. *J. Am. Chem. Soc.* **2010**, *18*, 6498–6506.
- [S18] Gao, P., Wang, X., Huang, Z., & Yu, H. *ACS Omega*. **2019**, *4*(7), 12385–12392.

## Appendix I NMR Spectra

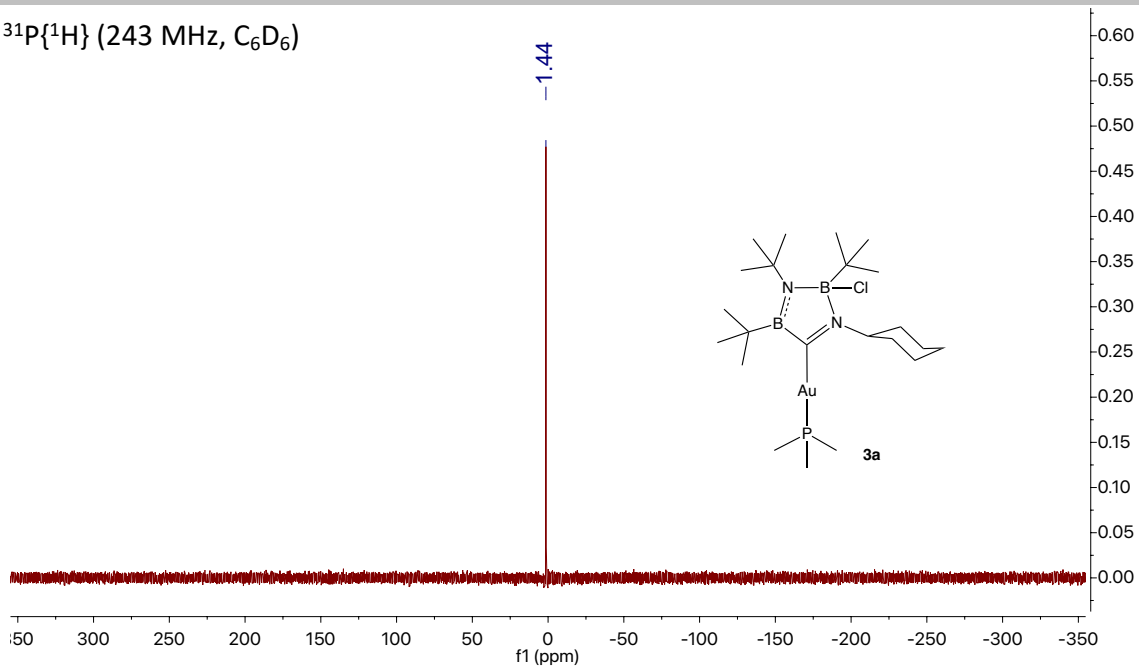
$^1\text{H}$  NMR Spectrum of **3a** (600 MHz,  $\text{C}_6\text{D}_6$ )



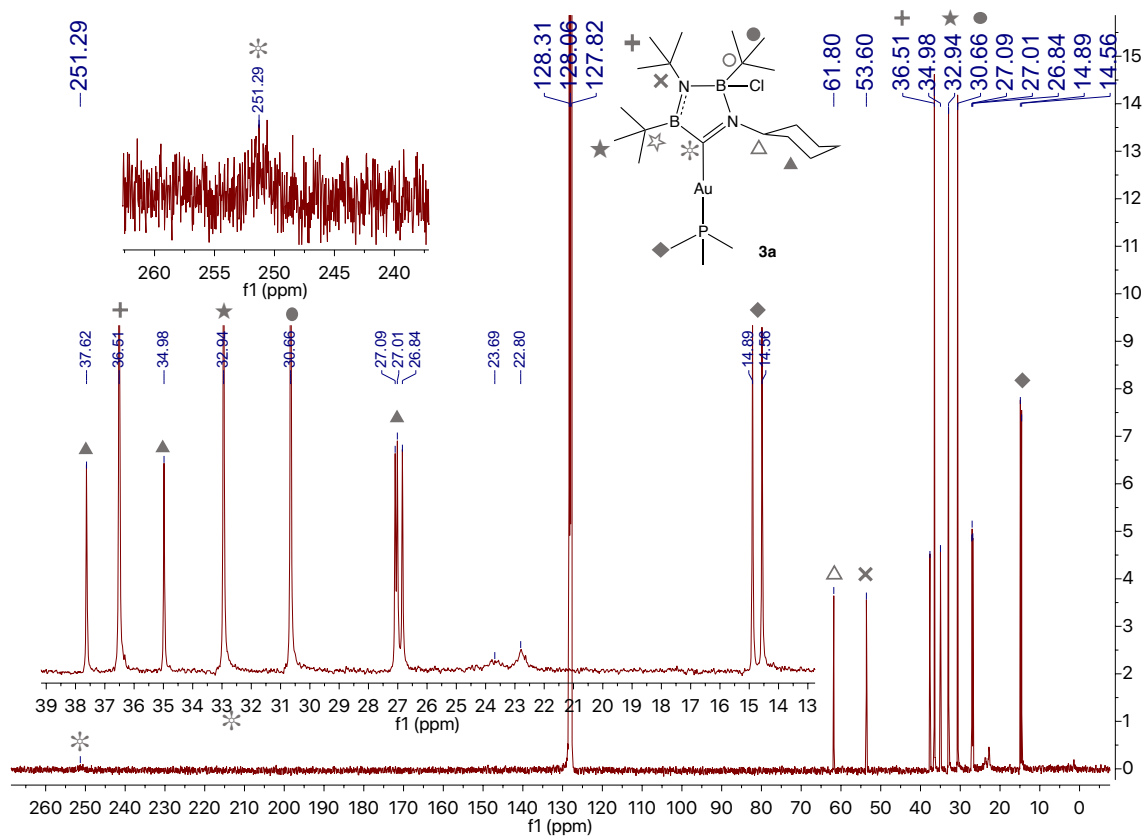
$^{11}\text{B}\{^1\text{H}\}$  NMR spectrum of **3a** (192 MHz,  $\text{C}_6\text{D}_6$ )



$^{31}\text{P}\{^1\text{H}\}$  (243 MHz,  $\text{C}_6\text{D}_6$ )

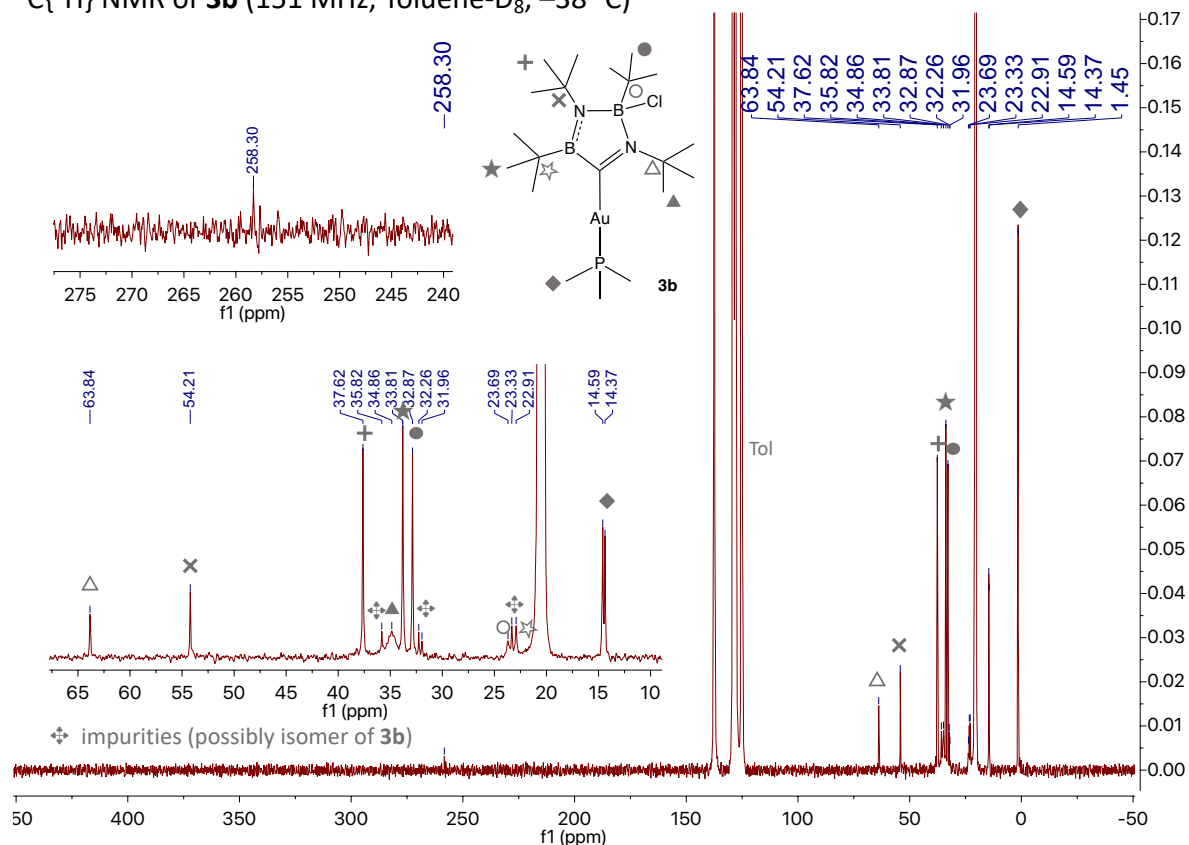


$^{13}\text{C}\{^1\text{H}\}$  NMR of **3a** (100 MHz,  $\text{C}_6\text{D}_6$ )

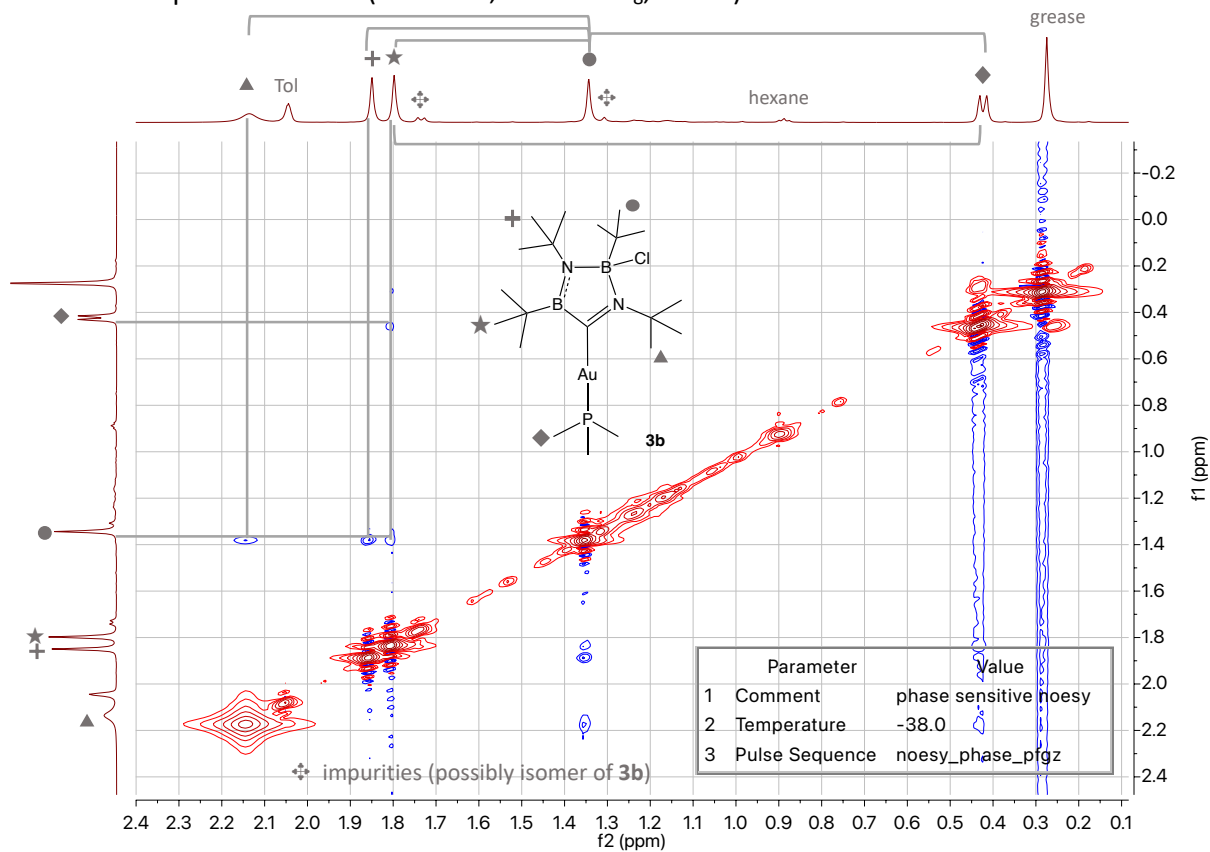




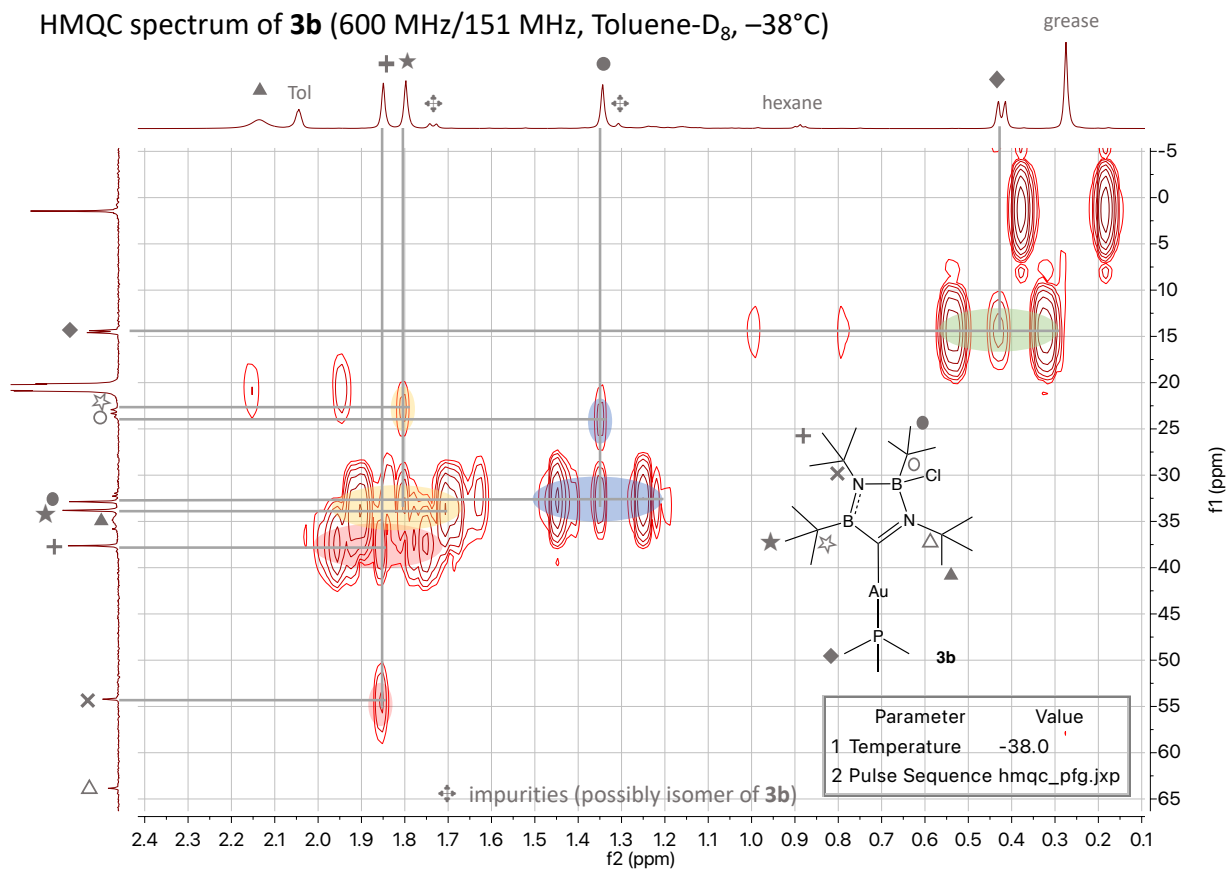
$^{13}\text{C}\{^1\text{H}\}$  NMR of **3b** (151 MHz, Toluene- $\text{D}_8$ ,  $-38^\circ\text{C}$ )



NOESY spectrum of **3b** (600 MHz, Toluene- $\text{D}_8$ ,  $-38^\circ\text{C}$ )

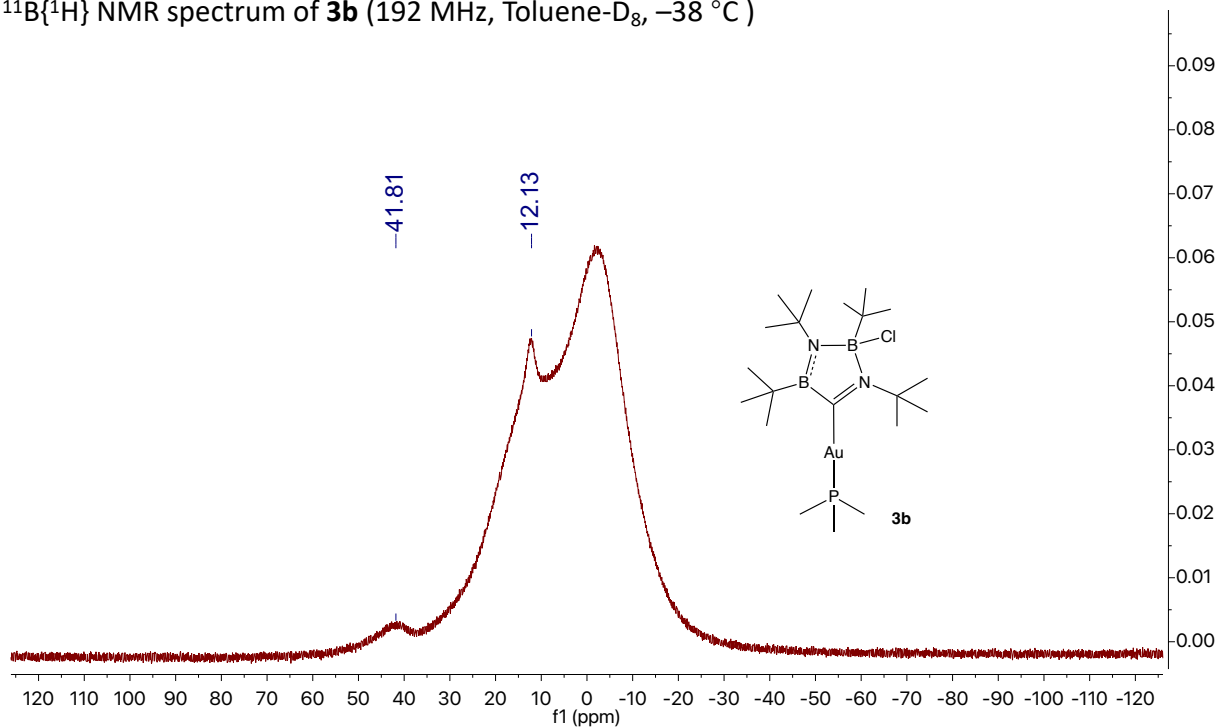


HMQC spectrum of **3b** (600 MHz/151 MHz, Toluene-D<sub>8</sub>, -38°C)

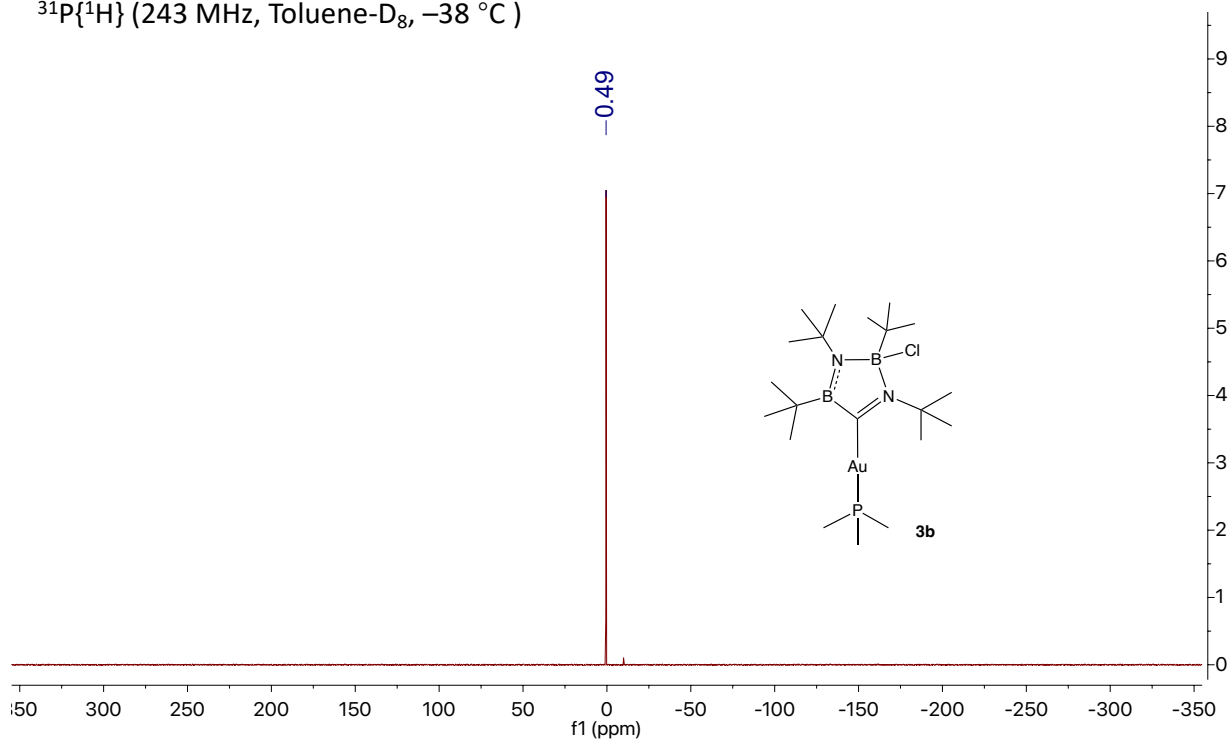


\*Both <sup>1</sup>J and <sup>2</sup>J H-C coupling were observed on this spectrum.

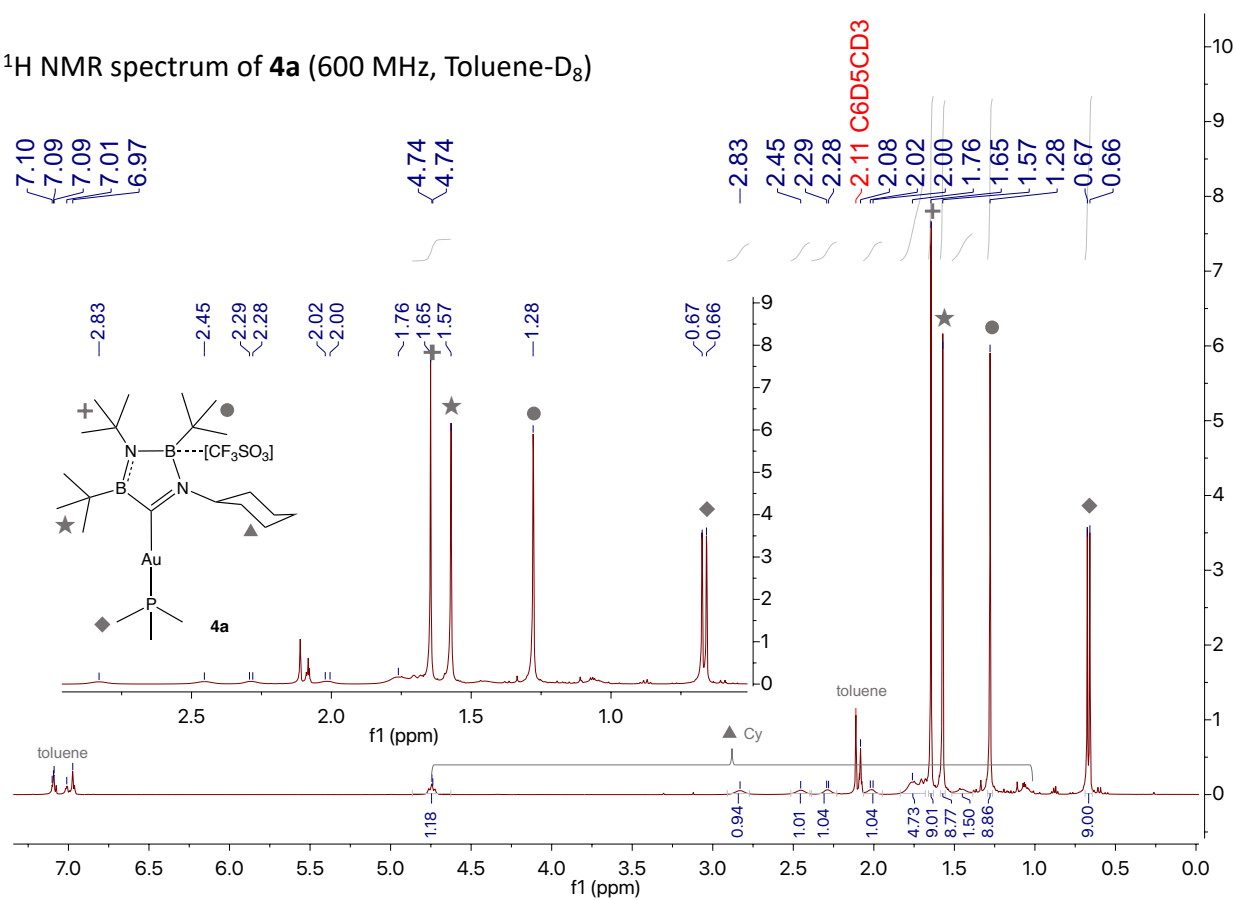
<sup>11</sup>B{<sup>1</sup>H} NMR spectrum of **3b** (192 MHz, Toluene-D<sub>8</sub>, -38 °C)



$^{31}\text{P}\{^1\text{H}\}$  (243 MHz, Toluene- $\text{D}_8$ ,  $-38^\circ\text{C}$ )

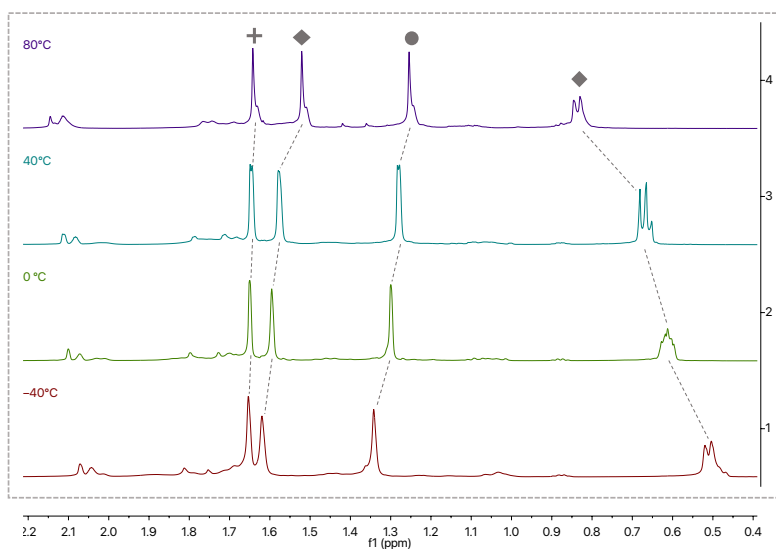
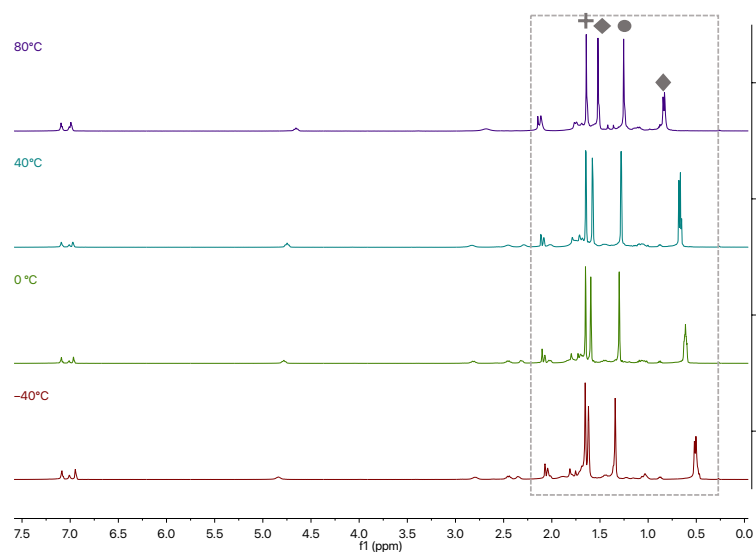


$^1\text{H}$  NMR spectrum of **4a** (600 MHz, Toluene- $\text{D}_8$ )

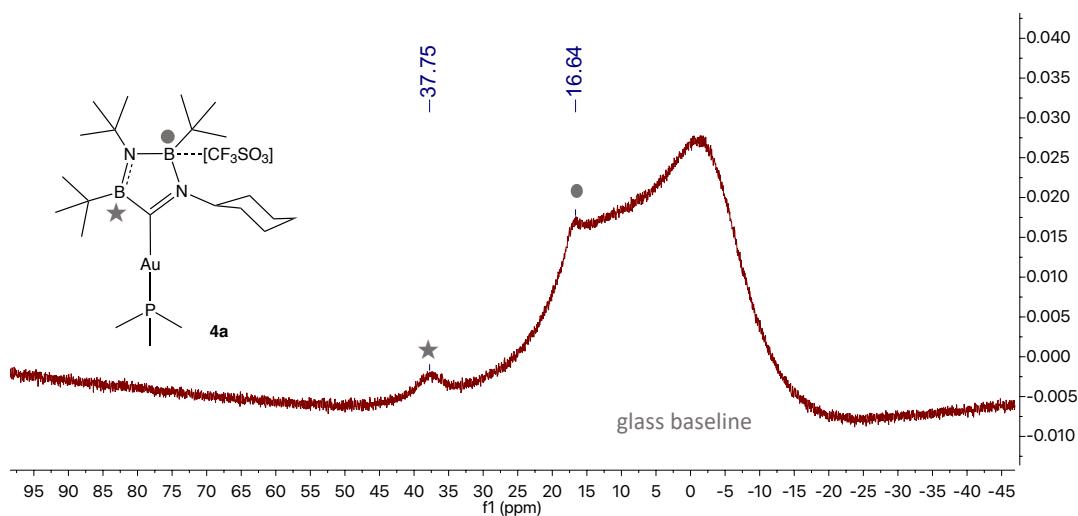




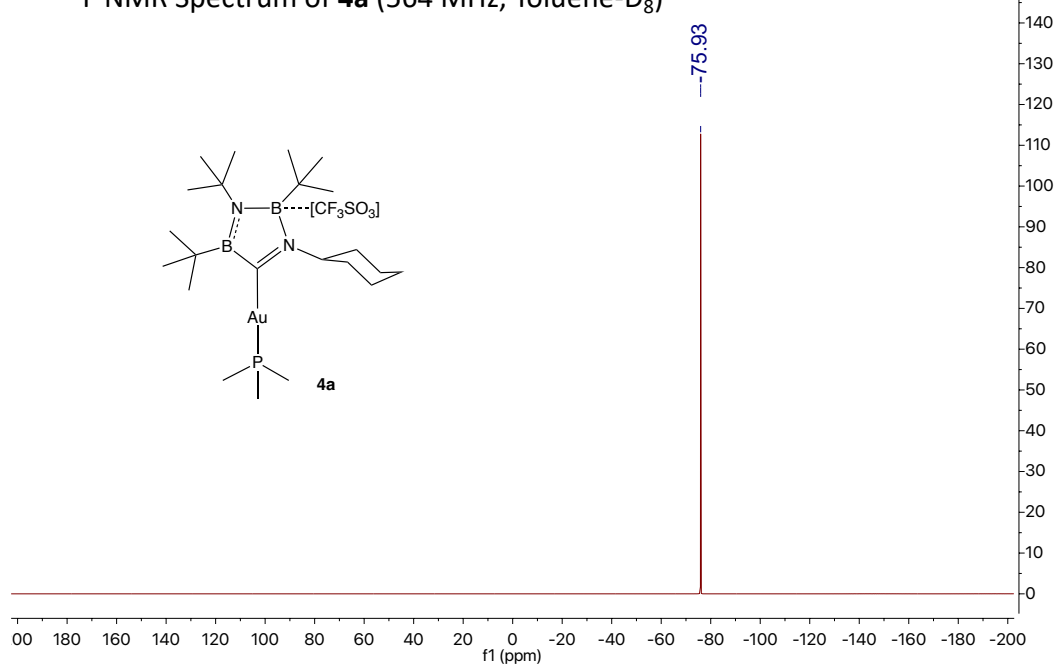
Variable Temperature  $^1\text{H}$  NMR spectra of **4a** (600 MHz, Toluene- $\text{D}_8$ )



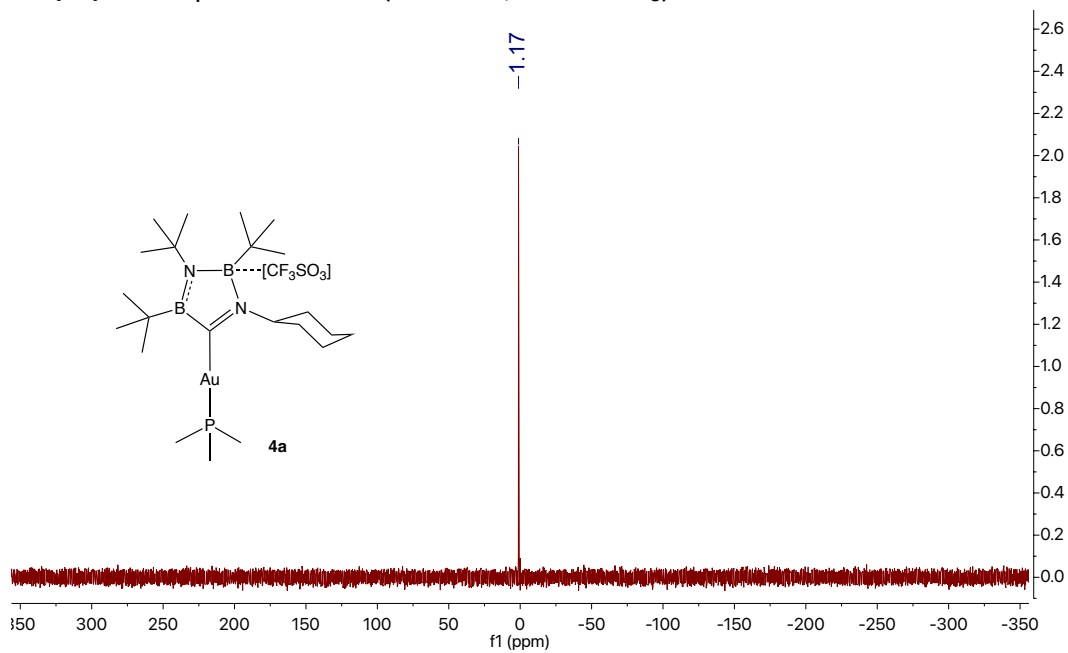
$^{11}\text{B}\{^1\text{H}\}$  NMR spectrum of **4a** (192 MHz, Toluene- $\text{D}_8$ )



$^{19}\text{F}$  NMR Spectrum of **4a** (564 MHz, Toluene- $\text{D}_8$ )

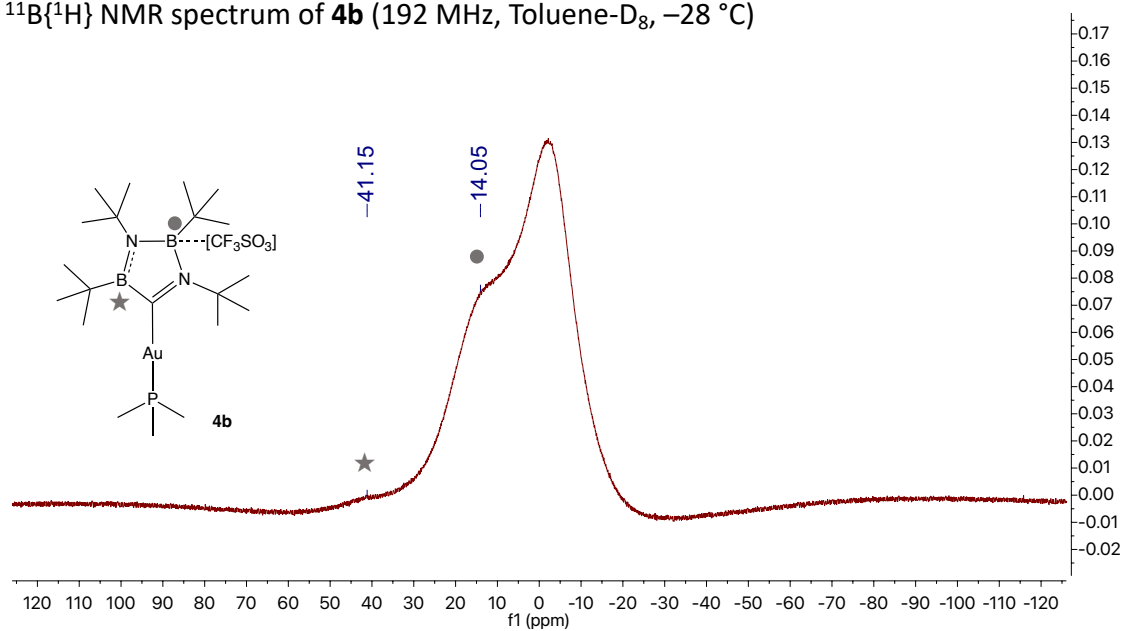


$^{31}\text{P}\{^1\text{H}\}$  NMR Spectrum of **4a** (243 MHz, Toluene- $\text{D}_8$ )

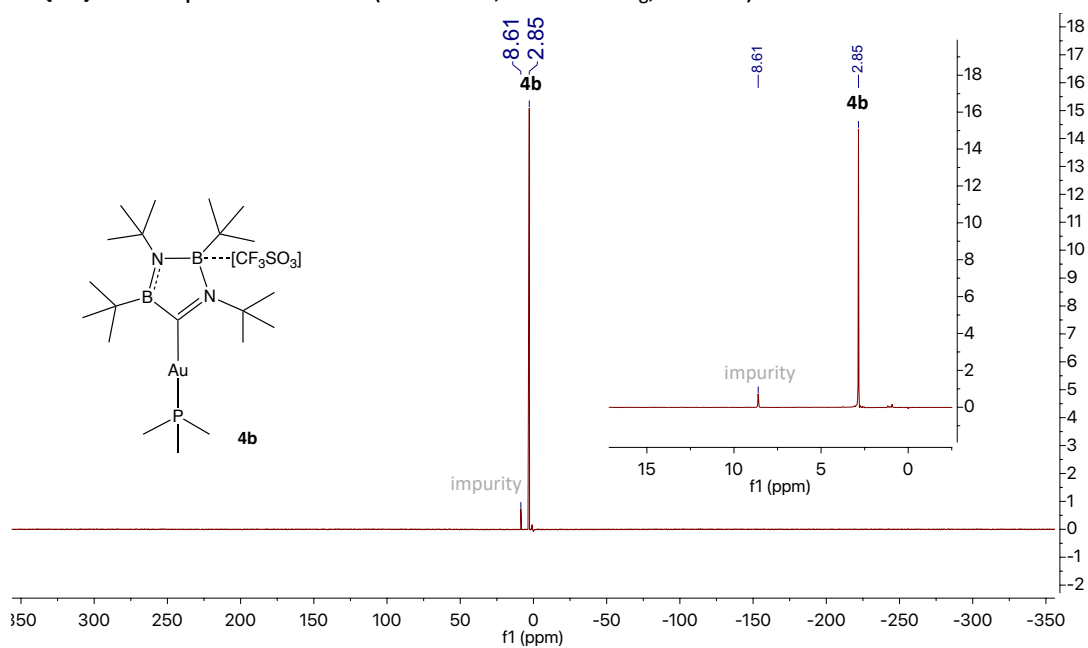




$^{11}\text{B}\{^1\text{H}\}$  NMR spectrum of **4b** (192 MHz, Toluene- $\text{D}_8$ ,  $-28^\circ\text{C}$ )

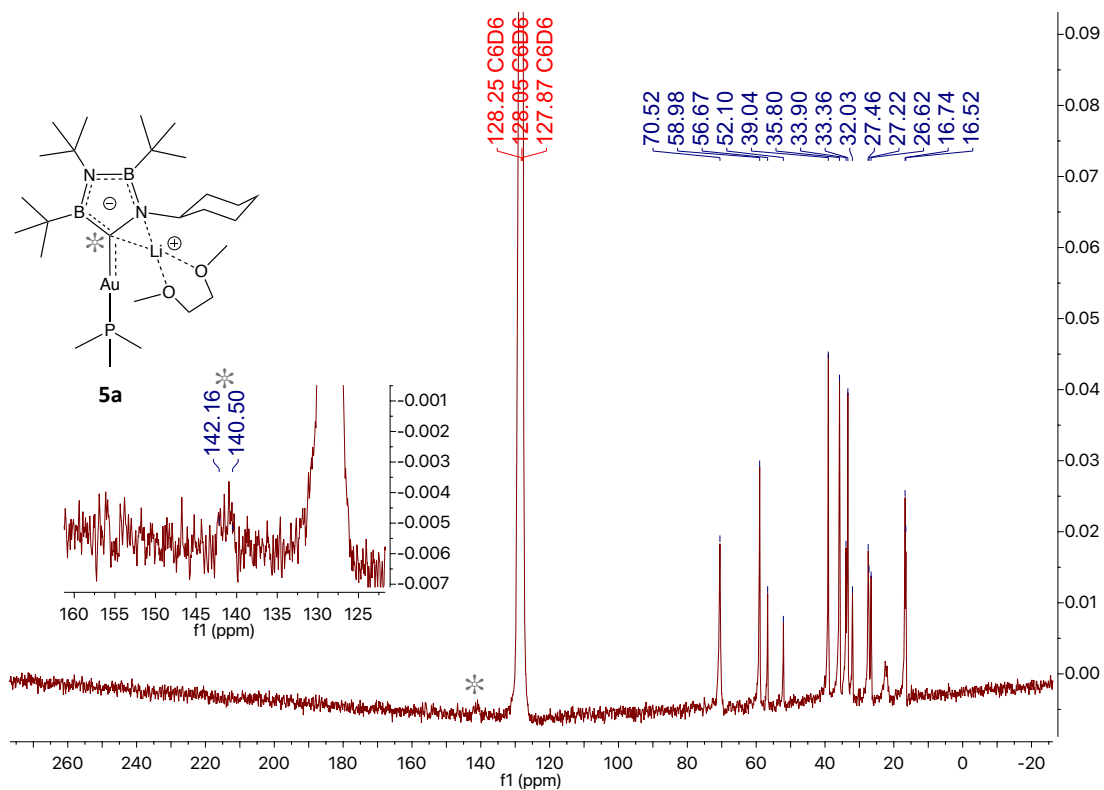


$^{31}\text{P}\{^1\text{H}\}$  NMR Spectrum of **4b** (243 MHz, Toluene- $\text{D}_8$ ,  $-28^\circ\text{C}$ )

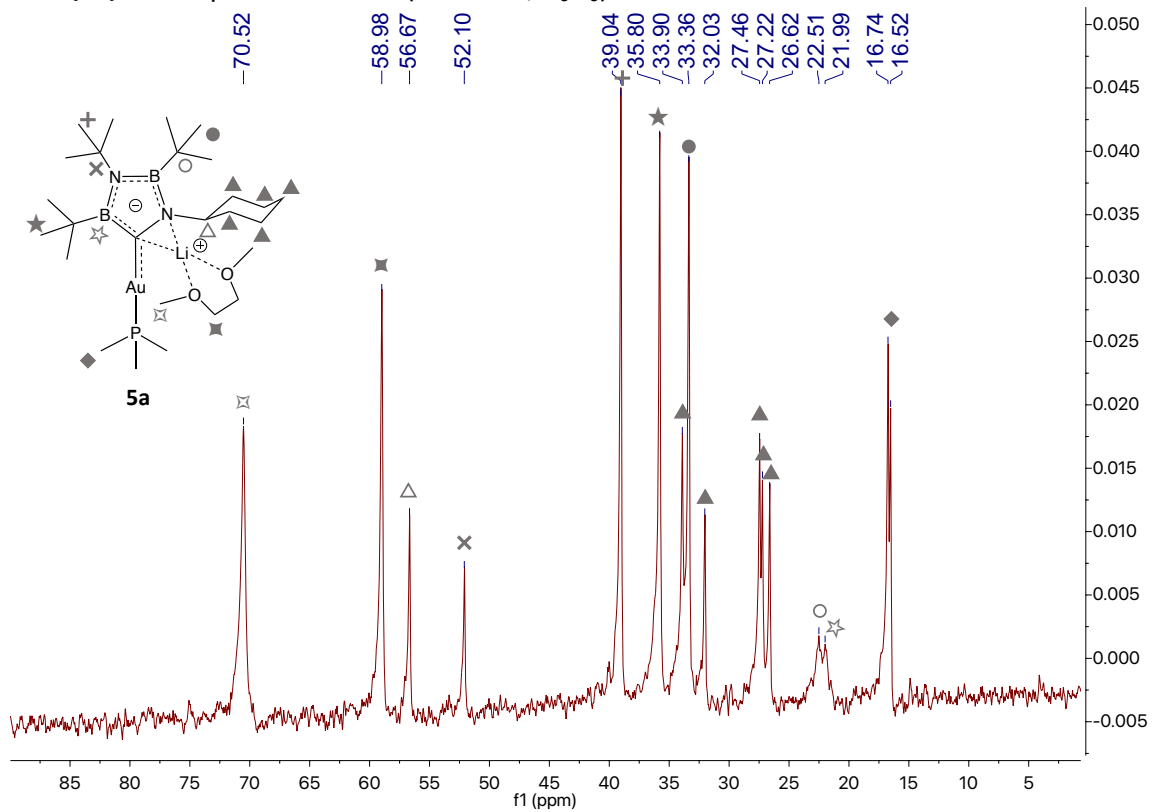


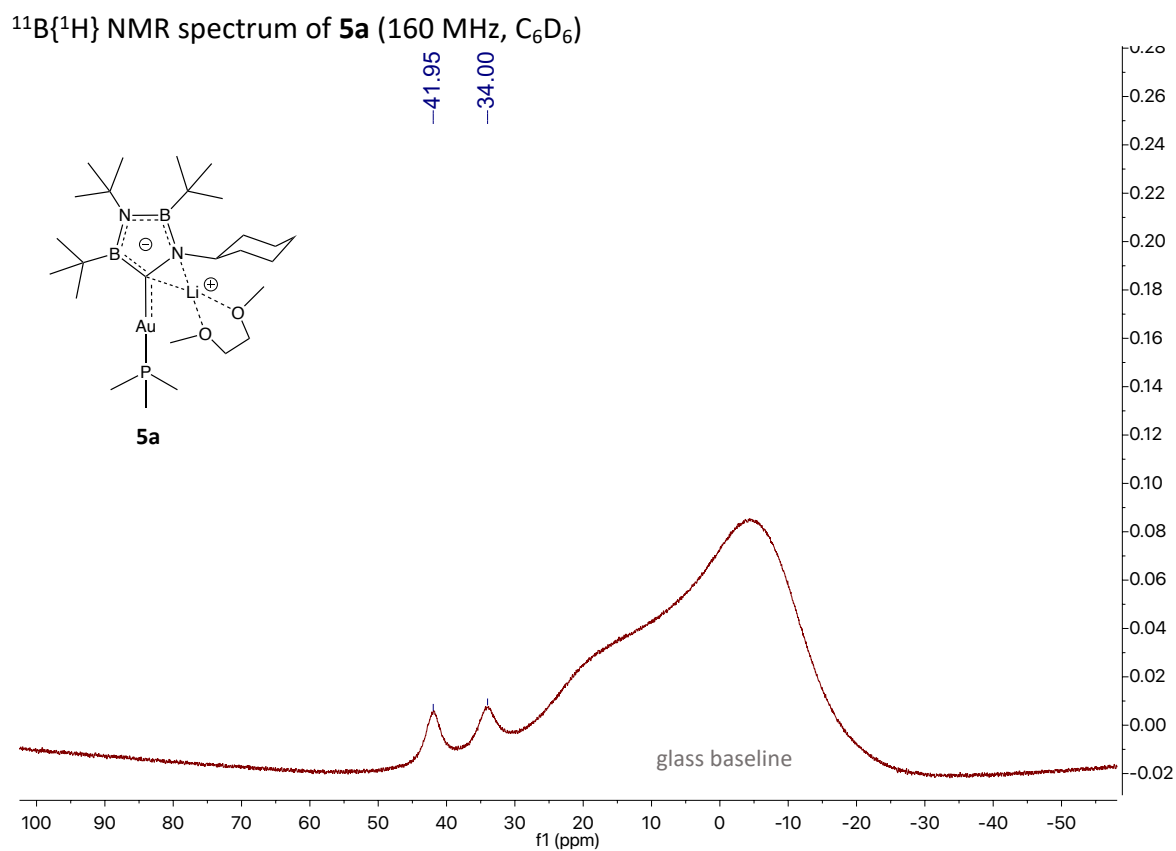
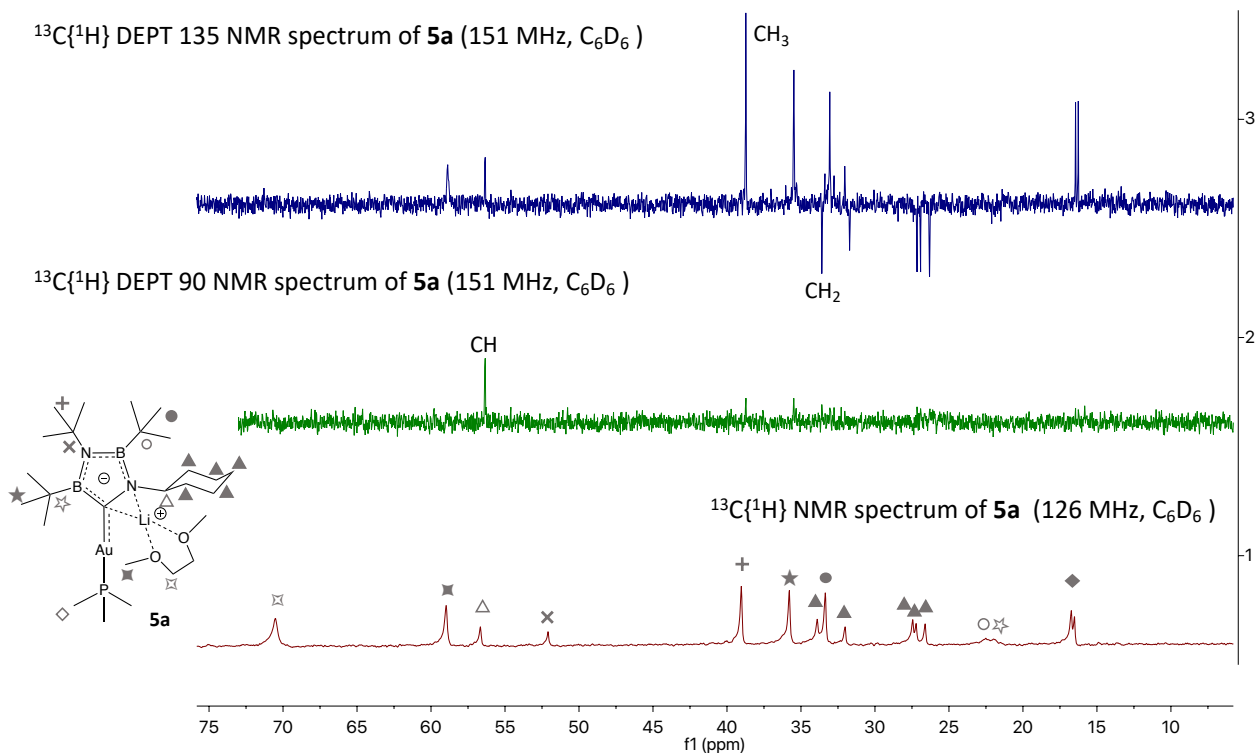


$^{13}\text{C}\{^1\text{H}\}$  NMR Spectrum for **5a** (126 MHz,  $\text{C}_6\text{D}_6$ )

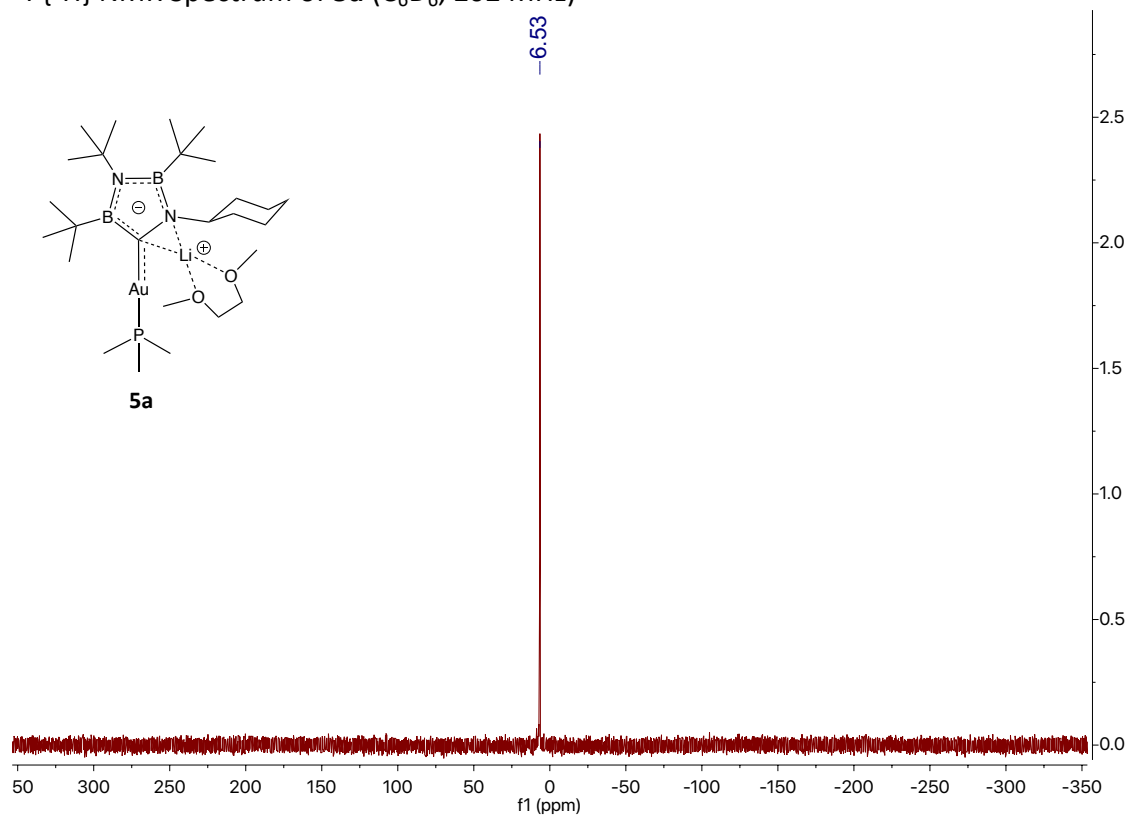


$^{13}\text{C}\{^1\text{H}\}$  NMR Spectrum for **5a** (126 MHz,  $\text{C}_6\text{D}_6$ )





$^{31}\text{P}\{^1\text{H}\}$  NMR Spectrum of **5a** ( $\text{C}_6\text{D}_6$ , 202 MHz)



$^7\text{Li}\{^1\text{H}\}$  NMR Spectrum of **5a** (194 MHz,  $\text{C}_6\text{D}_6$ )

